PLOS | PATHOGENS

RESEARCH ARTICLE

Norovirus infection results in eIF2α independent host translation shut-off and remodels the G3BP1 interactome evading stress granule formation

Michèle Brocard[1], **Valentina Iadevaia**[1], **Philipp Klein**[2], **Belinda Hall**[1], **Glenys Lewis**[1], **Jia Lu**[3], **James Burke**[4,5], **Margaret M. Willcocks**[1], **Roy Parker**[4,5], **Ian G. Goodfellow**[3], **Alessia Ruggieri**[2], **Nicolas Locker**[1]*

1 Faculty of Health and Medical Sciences, School of Biosciences and Medicine, University of Surrey, Guildford, United Kingdom, **2** Department of Infectious Diseases, Molecular Virology, Centre for Integrative Infectious Disease Research, University of Heidelberg, Heidelberg, Germany, **3** Division of Virology, Department of Pathology, University of Cambridge, Addenbrooke's Hospital, Hills Road, Cambridge, United Kingdom, **4** Department of Biochemistry, University of Colorado, Boulder, CO, United States of America, **5** Howard Hughes Medical Institute, University of Colorado, Boulder, CO, United States of America

* n.locker@surrey.ac.uk

OPEN ACCESS

Citation: Brocard M, Iadevaia V, Klein P, Hall B, Lewis G, Lu J, et al. (2020) Norovirus infection results in eIF2α independent host translation shut-off and remodels the G3BP1 interactome evading stress granule formation. PLoS Pathog 16(1): e1008250. https://doi.org/10.1371/journal.ppat.1008250

Editor: Stephanie M. Karst, University of Florida College of Medicine, UNITED STATES

Received: May 23, 2019

Accepted: December 4, 2019

Published: January 6, 2020

Copyright: © 2020 Brocard et al. This is an open access article distributed under the terms of the Creative Commons Attribution License, which permits unrestricted use, distribution, and reproduction in any medium, provided the original author and source are credited.

Data Availability Statement: The mass spectrometry proteomics data have been deposited to the ProteomeXchange Consortium via the PRIDE (Vizcaino et al., 2016) partner repository with the dataset identifier PXD011956.

Funding: Work in N.L.'s laboratory is supported by Biotechnology and Biological Sciences Research Council research grants [grant numbers BB/N000943/1, BB/P068018/1]. A.R. and P.K. were supported by the Deutsche

Abstract

Viral infections impose major stress on the host cell. In response, stress pathways can rapidly deploy defence mechanisms by shutting off the protein synthesis machinery and triggering the accumulation of mRNAs into stress granules to limit the use of energy and nutrients. Because this threatens viral gene expression, viruses need to evade these pathways to propagate. Human norovirus is responsible for gastroenteritis outbreaks worldwide. Here we examined how norovirus interacts with the eIF2α signaling axis controlling translation and stress granules. While norovirus infection represses host cell translation, our mechanistic analyses revealed that eIF2α signaling mediated by the stress kinase GCN2 is uncoupled from translational stalling. Moreover, infection results in a redistribution of the RNA-binding protein G3BP1 to replication complexes and remodelling of its interacting partners, allowing the avoidance from canonical stress granules. These results define novel strategies by which norovirus undergo efficient replication whilst avoiding the host stress response and manipulating the G3BP1 interactome.

Author summary

Viruses have evolved elegant strategies to evade host responses that restrict viral propagation by targeting the protein synthesis machinery and stress granules, which are membrane-less RNA granules with antiviral properties. Previous studies have unravelled how viruses, including norovirus the leading cause of gastroenteritis, regulate the activity of translation factors to affect the antiviral response. Furthermore, stress granules evasion strategies have been linked to targeting the scaffolding protein G3BP1. Here we dissect

Forschungsgemeinschaft (DFG, German Research Foundation) - Project number 272983813 - TRR179. IG is a Wellcome Senior Fellow [Ref: 207498/Z/17/Z] and also supported by the Biotechnology and Biological Sciences Research Council [grant number BB/N001176/1]. Funding for open access charge: Biotechnology and Biological Sciences Research Council. https://bbsrc.ukri.org; https://wellcome.ac.uk; https://www.dfg.de. The funders had no role in study design, data collection and analysis, decision to publish, or preparation of the manuscript.

Competing interests: The authors have declared that no competing interests exist.

how murine norovirus, the main model for norovirus, evades the cellular stress responses. Our work challenges the dogma that translational control during infection is mainly mediated by eIF2α and demonstrate that norovirus evades this stress pathway. We further show that norovirus evades the stress granule response in a novel way by isolating and characterising the G3BP1 interactome for the first time in the context of a viral infection. We conclude that norovirus infection results in a redistribution of G3BP1 and its cellular partners to replication complexes, thereby preventing the assembly of stress granules. Overall, we define a novel evasion strategy by which norovirus escapes stress granule formation by rewiring the G3BP1 interactome.

Introduction

The synthesis of viral proteins, whose functions are essential to viral replication and propagation, is wholly dependent on gaining control of the host cell translation machinery. However, the accumulation of double-stranded (ds) RNA replication intermediates or viral proteins imposes major stress on the host [1]. In response to this stress, infected cells can induce several defence mechanisms to promote cell survival and limit the use of energy and nutrients, which can culminate in a global reduction of protein synthesis, while paradoxically allowing the rapid synthesis of antiviral proteins [1–3]. Therefore, to replicate and spread, viruses need to balance their dependency on the host cell translation machinery with the adverse effect of antiviral proteins being synthesised by infected cells. As a consequence, interference with host mRNA translation represents a frequent evasion strategy evolved by viruses to subvert nearly every step of the host cell translation process [3, 4]. Most translational arrest strategies target translation initiation. This can be achieved by interfering with the initial cap-binding step mediated by eukaryotic initiation factor (eIF) 4F, targeting its integrity with viral proteases or its activity by modulating the mTOR or MAPK signaling pathways, or by altering the availability of the eIF2-GTP-$\mathrm{tRNA_i^{Met}}$ ternary complex by phosphorylating eIF2α [3, 4]. eIF2α phosphorylation is mediated by four kinases [5–9]. Among the four eIF2α kinases, protein kinase R (PKR) is activated by viral dsRNA sensing in the cytoplasm, however the other kinases: heme regulated eIF2α kinase (HRI), general control nonderepressible 2 (GCN2) and PKR-like ER localised kinase (PERK) can also be activated by infection cues such as oxidative stress, amino acid starvation and ER stress, respectively.

As consequence of translation initiation stalling and polysome disassembly, stalled mRNA initiation complexes can accumulate into membrane-less mRNA-protein granules called stress granules (SGs) [10]. While it remains poorly understood this is a process driven by aggregation prone RNA binding proteins such as Ras-GTPase activating SH3 domain binding protein 1 (G3BP1) and T cell internal antigen-1 (TIA-1), driving protein-protein and RNA-protein interactions that result in a liquid-liquid phase transition (LLPT) and assembly of SGs [11]. In addition, recently, RNA-RNA interactions have also been demonstrated to contribute to SG assembly [12, 13]. SGs are highly dynamic, able to rapidly assemble to act as storage sites for mRNAs, fuse and then dissolve upon stress resolution. The protein composition of SGs is highly variable and alters depending upon the type of stress induction [14–16]. In addition, while the bulk content of cytoplasmic mRNAs can be sequestered within SGs, specific exclusion of transcripts allows for stress-specific translational programme to combat stress [17, 18]. Furthermore SG or specific antiviral SGs (avSG) have been proposed to play a role in antiviral signaling as key signaling proteins including MDA5 and PKR are known to localise to SGs and SG formation is involved in PKR activation [19]. Although some may exploit SG for their replication many viruses have evolved strategies to antagonize SGs, by impairing the eIF2α sensing pathway or through the cleavage and sequestration of SG-nucleating proteins [20]. Among these, G3BP1 is prime target for several viruses as it is proteolytically cleaved by enterovirus and calicivirus proteases, sequestered by the alphavirus nsp3 protein or repurposed by the Dengue virus RNA and during vaccinia infection [20, 21]. Therefore viral infections have a profound impact on translational control, acting at the nexus between translation stalling and SG assembly.

The *Caliciviridae* family comprises small non-enveloped positive-strand RNA viruses of both medical and veterinary importance. Among these, human norovirus (HuNoV) is a leading cause of acute gastroenteritis and food-borne illnesses worldwide, accounting for nearly one fifth of cases and 200,000 deaths per annum [22, 23]. This also results in a significant economic burden to the health organisations with an estimated economic impact of $60 billion annually [24, 25]. The genogroup GII genotype 4 (GII.4) strains are responsible for the majority of outbreaks, including pandemics. While the diarrhoea and vomiting symptoms are acute and self-resolving in most children and adults, HuNoV has been reported to cause persistent infections, sometimes fatal, in the very young and elderly populations [26–28] and HuNoV infections exacerbates inflammatory bowel disease or has been associated with neonatal enterocolitis [29, 30]. Currently no specific vaccine or antiviral has been approved, and efforts to develop these have been hampered by the difficulty in culturing HuNoV *in vitro* and the lack of robust small animal models [31]. Recent studies have demonstrated that immortalised B cells and stem-cell derived intestinal organoids support HuNoV replication in culture, however these experimental systems are technically challenging and currently lack the degree of robustness required for a detailed analysis of the viral life cycle [31–33]. However, the related calicivirus murine norovirus (MNV) can be propagated in cell culture, has reverse genetics systems and small animal model and remains the main model for understanding the life cycle of caliciviruses [34, 35]. MNV and HuNoV share many characteristics such as their genome structure, environmental stability, faecal–oral transmission, replication in the gastrointestinal tract, and prolonged viral shedding [35]. Recently, the cell surface protein CD300lf was identified as a proteinaceous receptor for MNV [36]. Moreover, the expression of CD300lf alone in human cells is sufficient to enable MNV replication, suggesting the intracellular replication machinery for norovirus is conserved across species. MNV possesses a genome of ~7.5kb in length, capped by a viral genome-linked protein (VPg) covalently attached at the 5' end and polyadenylated at the 3' end. The VPg protein directs the translation of the MNV ORF1-4 by interacting directly with eIFs [37, 38] generating polyproteins subsequently proteolytically processed into three structural and seven non-structural proteins [39]. Meanwhile our previous studies have shown that MNV infection regulates translation in several ways by controlling the activity of multiple eIFs by inducing eIF4E phosphorylation via the MAPK pathway, and by cleavage of PABP and eIF4G by the viral protease or cellular caspases [37, 40]. Therefore, MNV induces hosts responses that affect translation and could coordinate SG assembly. Furthermore, while infection with another norovirus model, Feline Calicivirus (FCV) disrupts the assembly of SGs by inducing G3BP1 cleavage, MNV infection has no impact on G3BP1 integrity [41]. Herein, we address the complex interaction between MNV, the control of the host cell translation machinery and the SG response pathway. We show that while MNV infection impairs host cell translation early post-infection, this translational suppression is uncoupled from the activation of the eIF2α-dependent stress response and SG assembly. Instead, viral proteins interact with G3BP1 resulting in its re-localization to replication complexes and in the reshaping of its interactions with cellular partners that differ markedly from arsenite-induced granules. This provides evidence that MNV has evolved an evasion strategy to counteract the cellular SG response during infection.

Results

MNV infection results in hallmarks of translational stalling

To better understand the dynamic control of translation within infected cells, we addressed the global translational efficiency using single cell analysis by measuring the incorporation of puromycin, a tRNA structural mimic which specifically labels actively translating nascent polypeptides and causes their release from ribosomes [42, 43]. Anti-puromycin antibodies can then be used to detect puromycylated native peptide chains by confocal microscopy. To account for different cellular models used to study MNV replication, we chose to address this event in the murine macrophages cell lines RAW264.7 and primary murine bone marrow derived macrophages (BMDMs). Quantification of the puromycin signal intensity showed a significant decrease of protein synthesis following treatment with the translation elongation inhibitor cycloheximide (CHX) [44] in both RAW264.7 and BMDM cells (Fig 1A and 1B and Fig 1D and 1E). RAW264.7 and BMDM cells were infected with MNV and fixed at 6, 9 and 12h p.i. or 9 and 15h p.i, respectively. Quantification of the puromycin signal in individual infected cells, defined by immunostaining of MNV non-structural protein NS3, showed a progressive reduction in protein synthesis over time. In RAW264.7 and BMDM cells this decrease was detectable from 9h p.i onward. This time point correlated with peak viral protein production in direct comparison to cells infected with UV-inactivated MNV (MNV(UVi)) as a non-replicative control as evidenced by immunoblotting of RAW264.7 (from 2 to 10h p.i.) and BMDM (from 3 to 15h p.i.) cells (Fig 1C and 1F). These results extend our previous observations confirming that infection leads to a translation shut-off in cell lines permissive to MNV replication, and for the first time in primary cells [40].

During viral infection, the accumulation of double-stranded (ds) RNA replication intermediates commonly leads to the activation of the cytoplasmic pattern recognition receptor PKR, which results in the downregulation of the host translation machinery via phosphorylation of the translation initiation factor eIF2α, a hallmark of viral sensing [9]. Consequently, we then addressed the phosphorylation status of eIF2α in MNV-infected cells. Time course analysis by immunoblotting showed an accumulation of phosphorylated eIF2α (P-eIF2α) in MNV-infected cultures concomitant with the accumulation of viral products and translational shut-off but not in the cells inoculated with the UV-inactivated virus (Fig 1C and 1F). This result suggests that MNV replication triggers the expected host response to viral infection, through the activation of eIF2α phosphorylation, culminating in the host translation shut-off.

MNV-induced translational stalling is independent from the cellular stress response

While MNV has previously been shown to regulate the activity of the cap binding complex through targeting of PABP, eIF4G and eIF4E [40, 45], the increased eIF2α phosphorylation during infection prompted us to further investigate its role in MNV-induced translation suppression. The Integrated Stress Response Inhibitor (ISRIB) has previously been shown to reverse the inhibitory impact of P-eIF2α on its recycling factor eIF2B, allowing the exchange between GDP and GTP on phosphorylated substrates, thereby rescuing translation and resolving stress [46, 47]. To address the downstream activation of P-eIF2α pathway in MNV-infected cells, we measured the effect of ISRIB on translation shut-off and MNV replication. As expected, stimulation of RAW264.7 cells with tunicamycin, a known ER-stress inducer which activates the kinase PERK [48], resulted in a translational shut-off resolved by treatment of the cells with 200nM ISRIB (Fig 2A and 2B). However, in marked contrast, ISRIB treatment was unable to rescue the translational shut-off observed in MNV-infected cells at 10h p.i. (Fig 2A

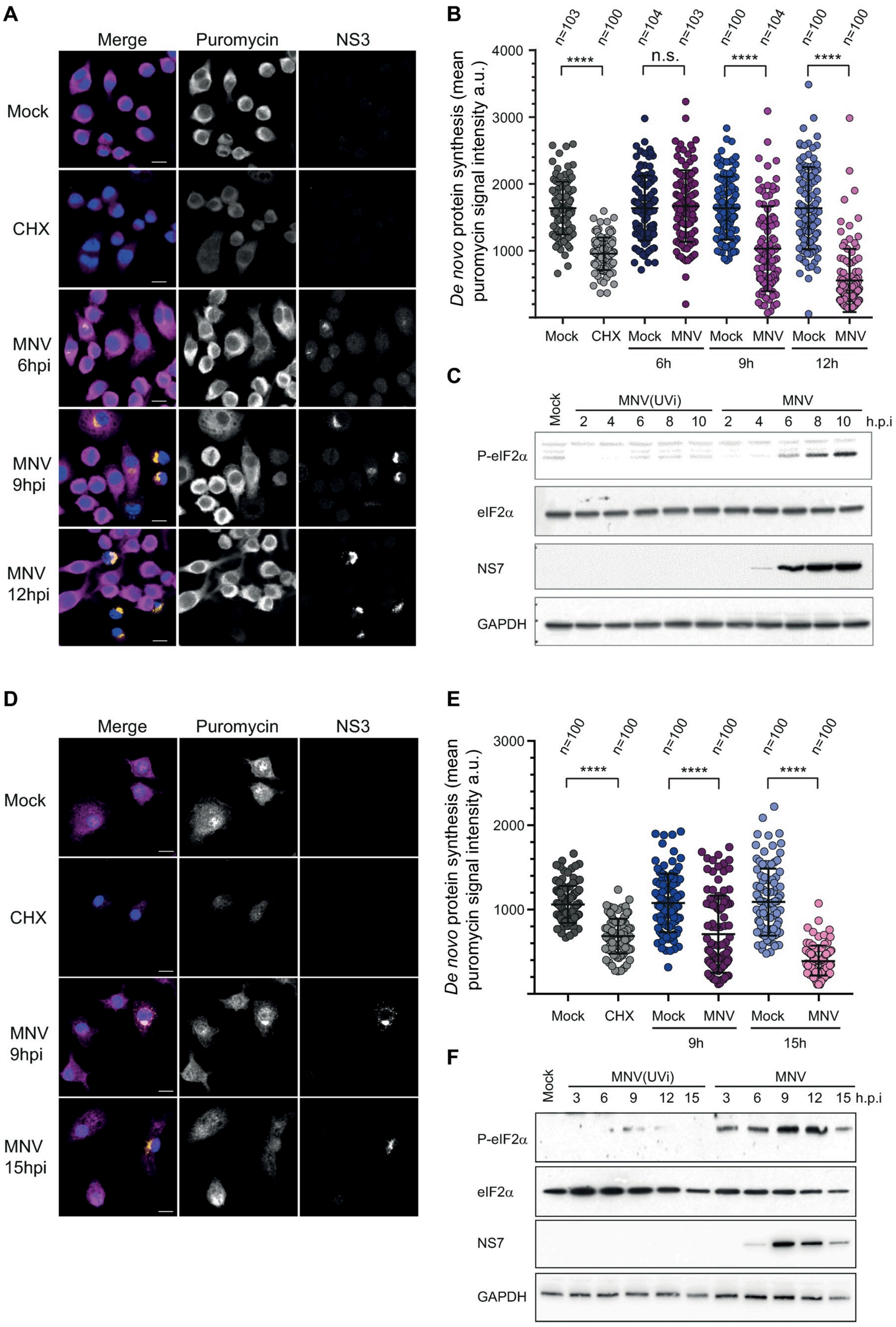
A
Merge
Puromycin
NS3
Mock
CHX
MNV 6hpi
MNV 9hpi
MNV 12hpi
B
De novo protein synthesis (mean puromycin signal intensity a.u.)
n=103
n=100
n=104
n=103
n=100
n=104
n=100
n=100
****
n.s.
****
****
4000
3000
2000
1000
Mock
CHX
Mock
MNV
Mock
MNV
Mock
MNV
6h
9h
12h
C
Mock
MNV(UVi)
MNV
2
4
6
8
10
2
4
6
8
10
h.p.i
P-eIF2α
eIF2α
NS7
GAPDH
D
Merge
Puromycin
NS3
Mock
CHX
MNV 9hpi
MNV 15hpi
E
De novo protein synthesis (mean puromycin signal intensity a.u.)
n=100
n=100
n=100
n=100
n=100
n=100
****
****
****
3000
2000
1000
Mock
CHX
Mock
MNV
Mock
MNV
9h
15h
F
Mock
MNV(UVi)
MNV
3
6
9
12
15
3
6
9
12
15
h.p.i
P-eIF2α
eIF2α
NS7
GAPDH

Fig 1. MNV replication results in gradual translational shut-off and hallmarks of eIF2α signaling activation in cell lines and primary cells. Decrease protein synthesis in MNV-infected RAW264.7 cells (A and B) or primary murine BMDMs (D and E). Naïve cells (Mock) or MNV-infected cells (MOI 10) for the indicated times were incubated with 10μg/ml of puromycin to label the nascent polypeptidic chains prior to fixation. CHX-treated cells were used as a negative control. Puromycin-labelled chains were visualised by immunostaining against puromycin (magenta) and infected cells were detected by immunostaining against MNV NS3 (gold). Nuclei were stained with DAPI. Representative views are shown for RAW264.7 cells (A) and BMDMs (D). Scale bars, 10μm. Representative scatter plots of *de novo* protein synthesis measured by fluorescence intensity of the puromycin signal (n = 3) in RAW264.7 cells (B) and BMDMs (E), a.u. arbitrary units. Statistical significance and number of analysed cells (n*)* are given at the top. **** $P < 0.0001$. MNV infection induces an increase of the phosphorylation levels of eIF2α (C and F). Representative Western Blot analysis (n = 3) of RAW264.7 cells (C) and BMDMs (F) infected (MOI 10) for the indicated times with replicative MNV or non-replicative virus MNV (UVi). Naive cells (Mock) were cultivated in parallel for 10h (C) or 15h (F).

https://doi.org/10.1371/journal.ppat.1008250.g001

and 2B). In addition, treatment with increased concentrations of ISRIB from 1 to 1000nM had no impact on viral replication as measured by $TCID_{50}$ assays (S1 Fig). These results suggest an uncoupling between eIF2α phosphorylation and translation suppression during MNV infection.

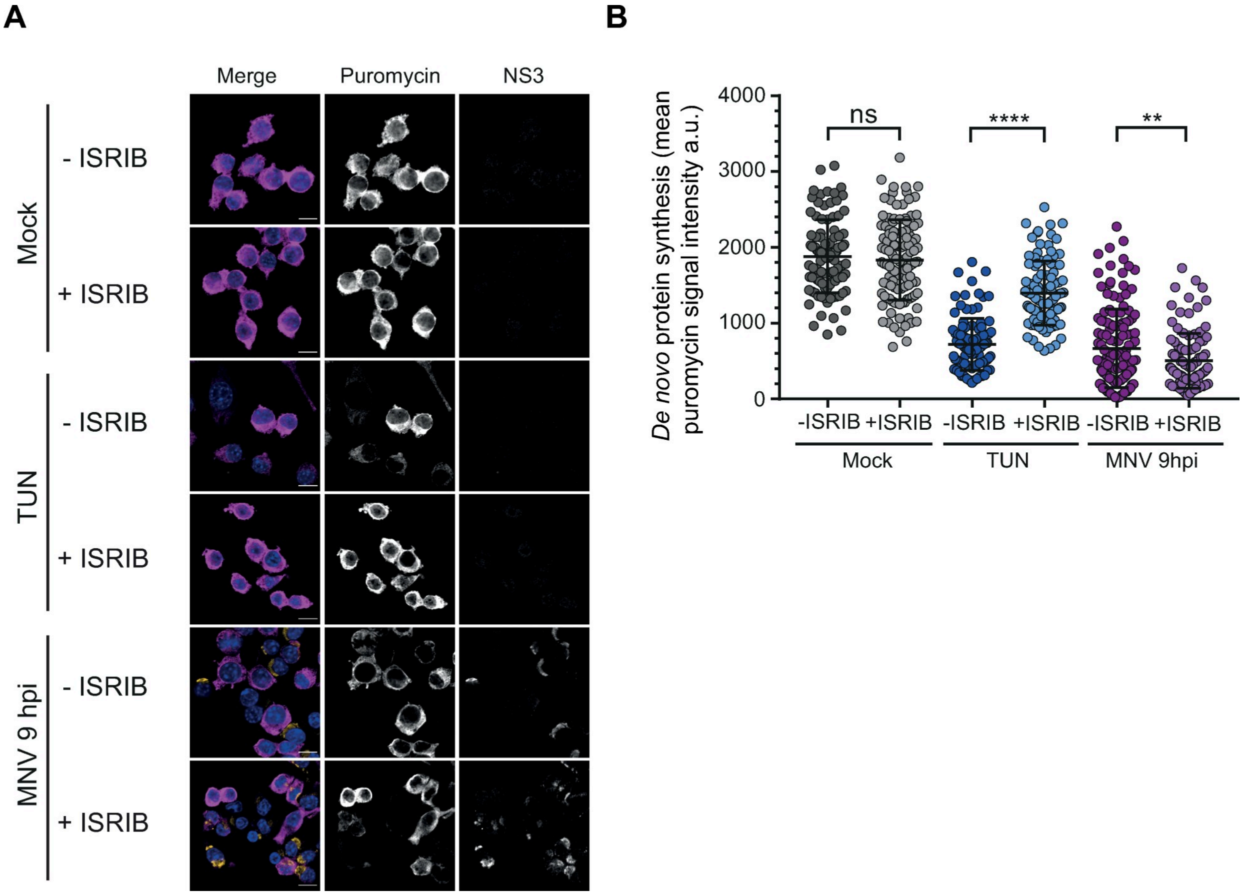

Fig 2. MNV-induced translation shut-off is uncoupled of P-eIF2α signalling. ISRIB treatment does not rescue MNV-induced translation shut-off (A and B). RAW264.7 cells were infected with MNV (MOI 10) for 10hp.i. or treated with 5μg/ml of tunicamycin (TUN) for 6h, with (+ISRIB) or without (-ISRIB) 200nM of ISRIB. Tunicamycin-treated cells were used as positive control for P-eIF2α-dependent translation shut-off. Cell cultures were incubated with 10μg/ml of puromycin to label the nascent polypeptidic chains. Puromycin-labelled chains were visualised by immunostaining against puromycin (magenta) and infected cells were detected by immunostaining against MNV NS3 (gold). (A) Representative views of the confocal analysis. Scale bars, 10μm. (B) Representative scatter plots of *de novo* protein synthesis measured by fluorescence intensity of the puromycin signal (n = 3), a.u. arbitrary units. Statistical significance and number of analysed cells (n*)* are given at the top. **** $P < 0.0001$, **, $P < 0.01$, n.s., no significance.

https://doi.org/10.1371/journal.ppat.1008250.g002

MNV infection leads to a metabolic-induced phosphorylation of eIF2α

To further understand the importance of eIF2α-dependent pathways during MNV infection, we engineered MEF cells expressing wild-type (wt) or a non-phosphorylable mutant of eIF2α (MEF S51A, [49]) to make them susceptible to MNV infection by constitutively expressing the MNV receptor CD300lf [36]. The accumulation of viral proteins by immunoblotting at 10h p.i. confirmed the ability of MNV to replicate in these cells (Fig 3A). Furthermore, the ability of MNV to produce infectious particles showed no difference between the wt and S51A MEFs as measured by viral yield assay (Fig 3B), suggesting that MNV replication is independent from eIF2α phosphorylation. Given that both the regulation of eIF4E and PABP activities were previously shown to contribute to MNV-induced translational shut-off [40, 45], we postulated this could occur independently from eIF2α phosphorylation. To address this, protein synthesis efficiency was quantified using ribopuromycylation assays in MEFs expressing S51A. When compared to wt MEFs, infection with MNV at 9h p.i. of S51A MEFs resulted in the expected reduction in global protein synthesis activity (Fig 3C and 3D). This confirmed that the phosphorylation of eIF2α during MNV infection is uncoupled from the observed translational shut-off.

Next, we interrogated the dynamic quantitative nature of eIF2α phosphorylation during MNV infection. To this end, we used Phos-tag acrylamide gel electrophoresis on a time course infection of RAW264.7 cells by MNV or MNV(UVi), allowing a direct quantification of the phosphorylated form compared to the total level of the protein using the same antibody on the same gel [50, 51]. As shown in S2 Fig, eIF2α is identified mainly as in two forms, the lower molecular mass product corresponding to the non-phosphorylated form and the weaker upper one corresponding to P-eIF2α. While no significant changes in eIF2α phosphorylation were observed during infection with MNV(UVi), infection with MNV resulted in a gradual increase in the amount of P-eIF2α from 3.53% to 11.37% at 10h p.i., compared to a maximum of 17.94% in arsenite-treated cells. Interestingly, this reveals that only a small fraction of the total eIF2α pool needs to be phosphorylated to result in the strong accumulation of SGs associated with arsenite-treatment, which is in agreement with recent observations that phosphorylation of 20% of eIF2α is sufficient to trigger SG formation and translation shut-off in HeLa cells [52].

During infection sensing of the viral dsRNA replication intermediates of RNA viruses by the pattern recognition receptors and eIF2α-kinase PKR is expected to trigger eIF2α phosphorylation [9]. Yet, the absence of correlation between eIF2α phosphorylation and translational efficiency, led us to question which of the four known kinases, all activated by different stresses, drives eIF2α phosphorylation during MNV infection (Fig 3E). In response to metabolic stresses such as UV irradiation and nutrients depletion, the kinase GCN2 has been shown to induce a phosphorylation of eIF2α as well as a P-eIF2α-independent translation shut-off [53, 54]. We therefore investigated the role of GCN2 activity on MNV-induced phosphorylation of eIF2α using the GCN2 inhibitor A-92 [55]. Increasing concentrations of A-92 added at 0h p.i. to MNV-infected RAW264.7 cells resulted in a dose-dependent inhibition of eIF2α phosphorylation, reduced to background levels (Fig 3F) suggesting GCN2 is responsible for this phosphorylation. To confirm the role of GCN2 in MNV-mediated eIF2α phosphorylation we measured eIF2α phosphorylation in wt or MEFs with a homozygous genetic deletion of GCN2 (GCN2 $^{-/-}$) [49] constitutively expressing the MNV receptor CD300lf. Both wt and GCN2 $^{-/-}$ MEFs responded to stimulation with arsenite, leading to eIF2α phosphorylation triggered by the kinase HRI (Fig 3G). In contrast, while UV irradiation and MNV infection induced eIF2α phosphorylation in wt MEFs, they resulted in an impaired response in GCN2 $^{-/-}$ MEFs with absence of eIF2α phosphorylation (Fig 3G). Overall these results suggest that the MNV-induced

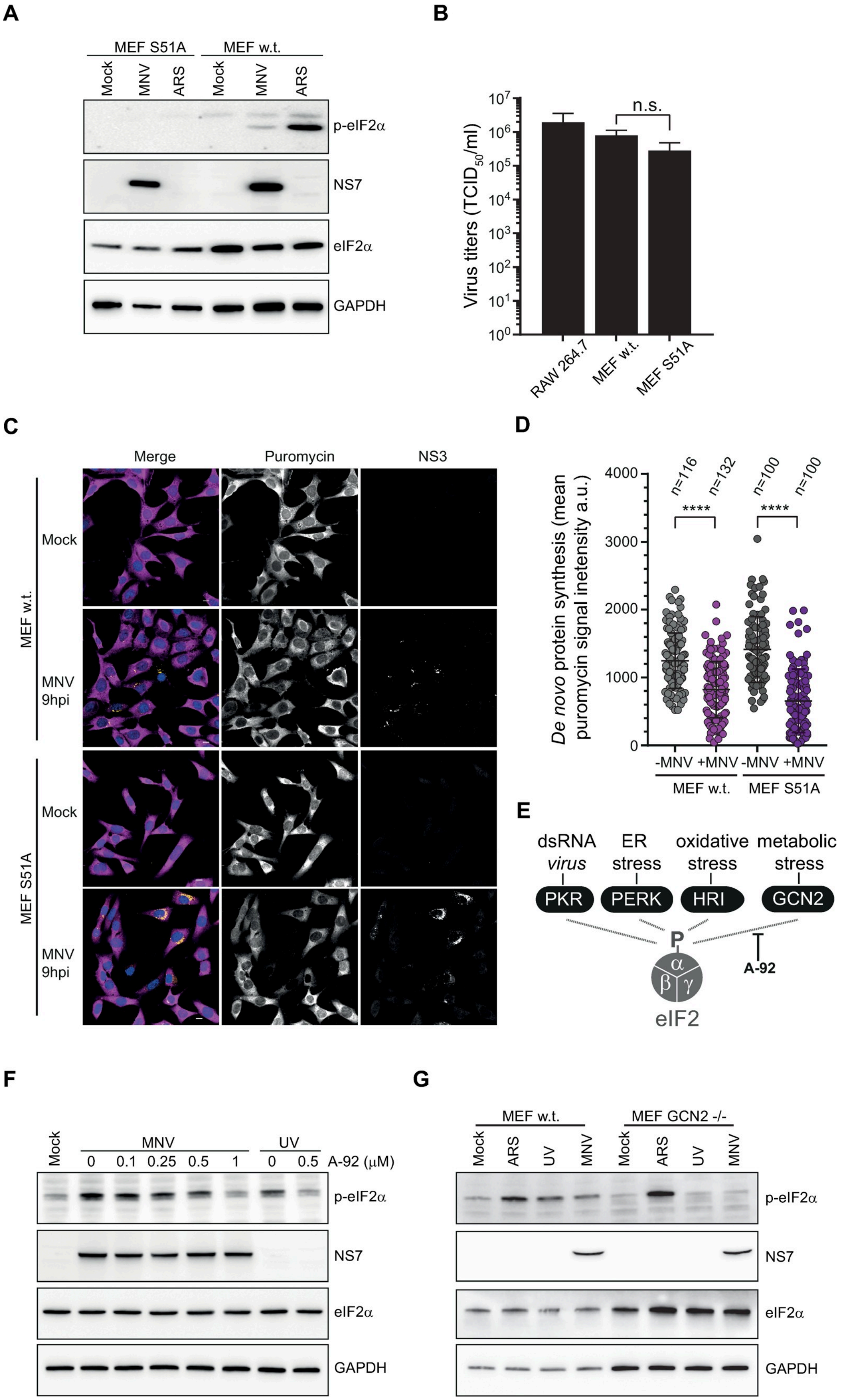
A
MEF S51A
MEF w.t.
Mock
MNV
ARS
Mock
MNV
ARS
p-eIF2α
NS7
eIF2α
GAPDH
B
Virus titers (TCID50/ml)
10^7
10^6
10^5
10^4
10^3
10^2
10^1
10^0
n.s.
RAW 264.7
MEF w.t.
MEF S51A
C
Merge
Puromycin
NS3
MEF w.t.
Mock
MNV 9hpi
MEF S51A
Mock
MNV 9hpi
D
De novo protein synthesis (mean puromycin signal inetensity a.u.)
4000
3000
2000
1000
0
n=116
n=132
n=100
n=100
****
****
-MNV
+MNV
-MNV
+MNV
MEF w.t.
MEF S51A
E
dsRNA virus
ER stress
oxidative stress
metabolic stress
PKR
PERK
HRI
GCN2
P
α
β
γ
eIF2
A-92
F
Mock
MNV
UV
0
0.1
0.25
0.5
1
0
0.5
A-92 (μM)
p-eIF2α
NS7
eIF2α
GAPDH
G
MEF w.t.
MEF GCN2 -/-
Mock
ARS
UV
MNV
Mock
ARS
UV
MNV
p-eIF2α
NS7
eIF2α
GAPDH

Fig 3. MNV-induced P-eIF2α is uncoupled from translational shut-off and is dependent upon GCN2 activity. P-eIF2α is dispensable for MNV infection (A and B). Wild type (w.t.) or expressing unphosphorylatable eIF2α (S51A) MEF cells, constitutively expressing MNV receptor CD300lf were infected with MNV (MOI 10) for 10hp.i. Arsenite-treated cells were used as control. (A) Representative western blot analysis (n = 2) of the translation of MNV NS7 in absence of P-eIF2α. P-eIF2α has no effect on MNV replication in MEF (B). Bar plots of the viral titre measured by TCID50 (logarithmic scale) from MEF(w.t.) and MEF(S51A) infected with MNV (MOI 1) for 16h. RAW264.7 cells were used as control. Mean ±SD (n = 3), statistical analysis given above the bars, n.s, not significant. MNV-induced translation shut-off is independent of P-eIF2α (C and D). Uninfected (Mock) or MNV-infected MEF(w.t.) and MEF (S51A) cells (MOI 10) for 9h p.i. were incubated with 1μg/ml of puromycin to label the nascent polypeptidic chains. Puromycin-labelled chains were visualised by immunostaining against puromycin (magenta) and infected cells were detected by immunostaining against MNV NS3 (gold). (C) Representative views of the confocal analysis, scale bars, 10μm. (D) Representative scatter plots (n = 2) of *de novo* protein synthesis measured by fluorescence intensity of the puromycin signal of uninfected (-MNV) and MNV-infected (+MNV) cells, a.u. arbitrary units. Statistical significance and number of analysed cells (n*)* are given at the top, **** $P < 0.0001$. MNV-induced P-eIF2α is dependent upon GCN2 activity (E, F and G). (E) Diagram of the pathways leading to the phosphorylation of eIF2α and showing the inhibition of GCN2 by A-92. (F) Representative western blot analysis (n = 2) of RAW264.7 cells, naïve (Mock) or infected with MNV for 10hp.i. (MOI 10) in presence of increasing doses of A-92 ranging from 0.1μM to 1μM (MNV). UV-irradiated RAW264.7 cells were used as control, cultivated in parallel and treated with 0.5μM of A-92 (UV). (G) Representative western blot analysis (n = 2) of MEF(w.t.) and MEF(GCN2-/-) constitutively expressing MNV receptor CD300lf, naïve (Mock) or infected with MNV for 10hp.i. (MOI 10). Arsenite treated cells (ARS) were used as positive control for phosphorylation of eIF2α and UV-irradiated cells as positive control for GCN2 activity (UV).

https://doi.org/10.1371/journal.ppat.1008250.g003

translational shut-off occurs independently from eIF2α phosphorylation, which itself is driven by GCN2 activation rather than PKR-mediated sensing of viral RNA.

MNV infection does not induce canonical stress granule assembly

The inhibition of translation initiation via eIF2α-dependent or independent pathways during infection is intimately linked to the assembly of SGs [1]. To counteract this stress response, many viruses have evolved strategies to impair SG formation [20]. We previously reported that FCV prevents SG formation through the cleavage of the nucleating factor G3BP1 by the viral proteinase NS6^{Pro}, while we observed no impact of MNV infection on G3BP1 integrity in the J774A.1 murine macrophages cell line [41]. To better examine a potential role for the activation of the stress response in MNV-induced translational suppression and to better understand the interaction of noroviruses with SGs, we analysed SG formation in more detail. (Fig 4).

Most known SG markers, such as TIA-1, G3BP1 or Caprin1, were found unsuitable for immunofluorescence analysis in RAW264.7 cells with poor SG detection following arsenite treatment. Therefore for our studies we used the murine microglial cell line BV2 stably over-expressing an exogenous GFP-tagged G3BP1 (BV2 GFP-G3BP1), allowing us to detect the subcellular distribution of total G3BP1 by immunofluorescence microscopy. In addition to G3BP1, the eukaryotic initiation factor eIF3B was also used as a *bona fide* SG marker, and the viral protein NS3 as a marker for infected cells. First, we confirmed that this cell line was as permissive to MNV infection as the non-transfected parental line by assessing the viral titers following infection at a MOI of 1 (S3 Fig). While no SG were detected in uninfected cells, upon treatment of BV2 GFP-G3BP1 for 1h with 0.5mM arsenite, which induces oxidative stress and eIF2α-dependent inhibition of translation, both G3BP1 and eIF3B relocated to SGs (Fig 4A). In stark contrast, infection with MNV for 9h resulted in the accumulation of G3BP1 in large cytoplasmic foci localized closely to the nucleus and colocalising with an accumulation of the viral protein NS3. The foci identified were devoid of eIF3B suggesting that they did not represent canonical SGs. Noteworthy, these structures highly resemble previously characterized MNV replication complexes [56–58]. Analysis of earlier time points at 2, 4, 6 or 8h post infection confirmed this with complete absence of G3BP1 and eIF3B positive SGs during MNV infection (S4A and S4B Fig). To ensure that this was not an experimentally induced artefact as a result of GFP-G3BP1 over-expression, we confirmed that the endogenous G3BP1

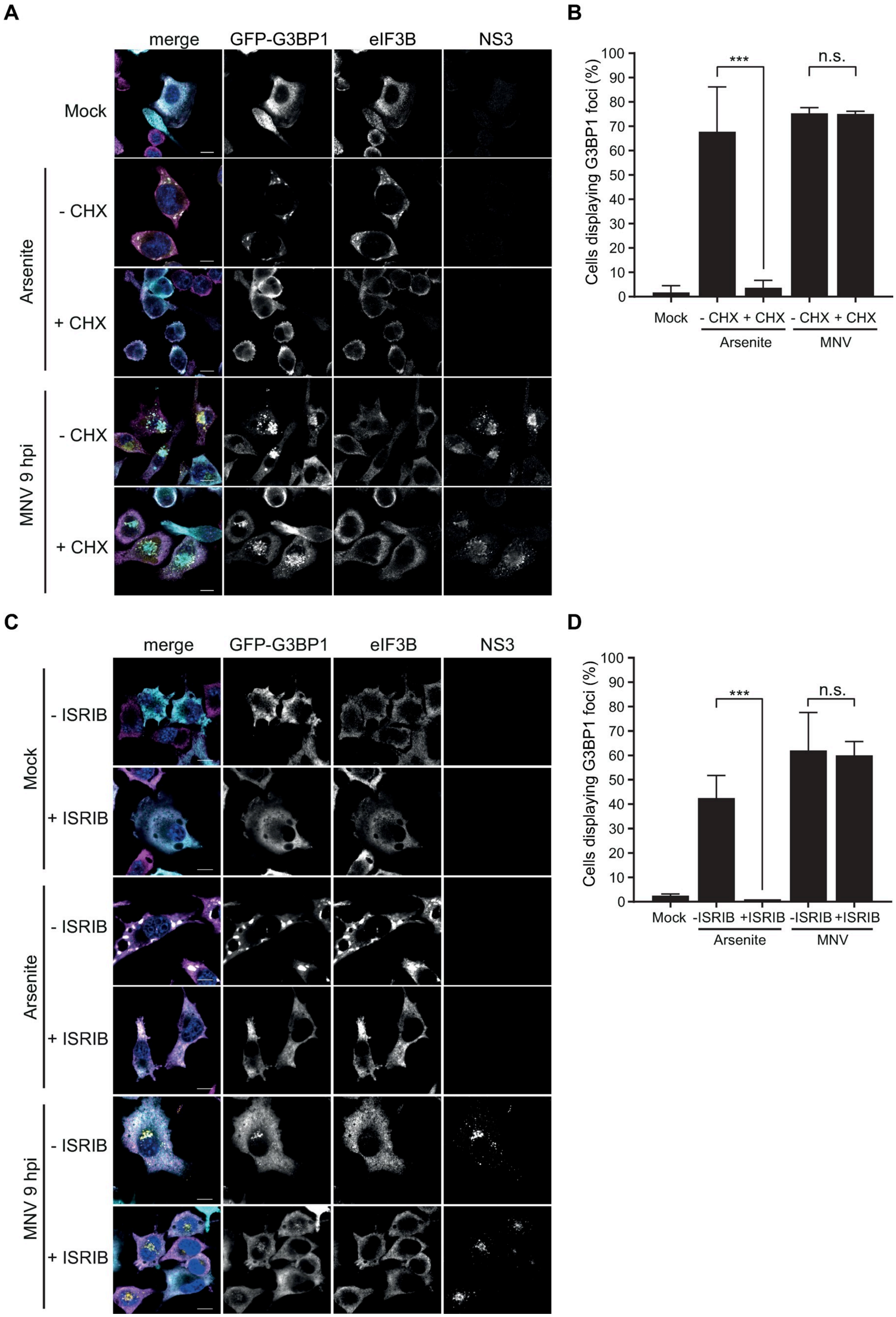
A
merge
GFP-G3BP1
eIF3B
NS3
Mock
Arsenite
- CHX
+ CHX
MNV 9 hpi
- CHX
+ CHX
B
Cells displaying G3BP1 foci (%)
100
90
80
70
60
50
40
30
20
10
0
***
n.s.
Mock
- CHX
+ CHX
- CHX
+ CHX
Arsenite
MNV
C
merge
GFP-G3BP1
eIF3B
NS3
Mock
- ISRIB
+ ISRIB
Arsenite
- ISRIB
+ ISRIB
MNV 9 hpi
- ISRIB
+ ISRIB
D
Cells displaying G3BP1 foci (%)
100
90
80
70
60
50
40
30
20
10
0
***
n.s.
Mock
-ISRIB
+ISRIB
-ISRIB
+ISRIB
Arsenite
MNV

Fig 4. MNV infection results in the assembly of non-canonical cytoplasmic G3BP1 granules. MNV-induced G3BP1 aggregates are CHX insensitive (A and B). BV2 GFP-G3BP1 cells were infected with MNV (MOI 10) for 9h p.i. arsenite-treated cells were used as positive control for SG formation. For forced SG disassembly, cells were treated with 10μg/ml of CHX for 30min (+CHX). (A) Confocal analysis of the formation of MNV-induced granules in GFP-G3BP1 (cyan) positive cells. Samples were stained for the SG marker eIF3B (magenta) and infected cells detected by immunostaining against MNV NS3 (gold). Scale bars, 10μm. (B) Representative bar plot (n = 3) of the percentage of cells displaying GFP-G3BP1 foci, mean ± SD for 100 GFP-positive cells (Mock and arsenite) and GFP- and NS3-positive cells (MNV) analysed across at least 10 acquisitions. Statistical significance shown above the bars, ***, $P < 0.001$, n.s., not significant. MNV-induced G3BP1 granules are insensitive to ISRIB treatment (C and D). BV2 GFP-G3BP1 cells were infected with MNV (MOI 10) for 9hp.i. or treated with 0.1mM of arsenite (ARS) for 45 min, with (+ISRIB) or without (-ISRIB) 200nM of ISRIB. Arsenite-treated cells were used as positive control for SG formation. (C) Representative views of confocal analysis (n = 3) of the subcellular distribution of GFP-G3BP1 (cyan), counterstaining of stress granules by immunodetection of eIF3B (magenta) and detection of the infected cells by immunostaining against MNV NS3 (gold). Nuclei were stained with DAPI. Scale bars, 10μm. (D) Bar plots of the number of cells displaying GFP-G3BP1 foci as a percentage of the GFP-positive cells (Mock and arsenite) or GFP- and NS3-positive cells (MNV), mean ±SD (n = 3). Statistical significance given above the bars, ***, $P < 0.001$, n.s., no significance.

https://doi.org/10.1371/journal.ppat.1008250.g004

redistributed in a similar manner, both in cell lines and primary cells (S5A and S5B Fig). Furthermore, another SG component eIF3E was excluded from MNV-induced G3BP1 foci in BV2 cells constitutively expressing both GFP-G3BP1 and mCherry-eIF3E (S5C Fig).

SGs are assembled by phase separation of stalled mRNA transcripts that accumulated in the cytosol upon polysome disassembly. Therefore, the translation elongation inhibitor CHX, by trapping the ribosomes on mRNA transcripts, prevents the accumulation of stalled initiating complexes required for the formation of SGs and is used to discriminate between canonical SGs and other cytoplasmic granules [59]. Treatment of BV2 GFP-G3BP1 cells with CHX resulted in a potent block of SG assembly upon treatment with arsenite (Fig 4A and 4B). In contrast, CHX treatment had no significant impact on the accumulation of G3BP1 granules at 9h p.i. and its co-localisation with NS3 (Fig 4A and 4B). Next, we addressed the impact of P-eIF2α signaling by measuring the effect of ISRIB on G3BP1 localisation. As expected, treatment of the cells with 200nM ISRIB resolved the accumulation of stress granules induced by arsenite in BV2 GFP-G3BP1 cells (Fig 4C and 4D). However, ISRIB treatment had no impact on the accumulation of G3BP1 granules during MNV infection (Fig 4C and 4D). Altogether, these results suggest that MNV infection leads to a redistribution of G3BP1, which is not driven by the accumulation of stalled initiating complexes and is uncoupled from eIF2α signaling.

G3BP1 colocalizes with viral replication complexes during MNV infection

Viral replication complexes of RNA viruses are observed as cytoplasmic foci characterized by the co-localisation of non-structural proteins required for the replication of the genomic RNA and viral dsRNA replication intermediates. Single cell analysis of the subcellular distribution of dsRNA in MNV-infected BV2 GFP-G3BP1 cells at different times post-infection showed a strong colocalisation of both NS3 and dsRNA in the juxtanuclear structures previously shown in Fig 4, further defining them as potential MNV replication centers (Fig 5A). Remarkably, those structures also contain GFP-G3BP1 and are discernable as early as 6h p.i. and at 9h p.i, suggesting the recruitment of G3BP1 to MNV replication complexes is concomitant with the accumulation of viral products. Of note, the redistribution of G3BP1 to this juxtanuclear structure does not occur in arsenite-treated cells indicating that this accumulation is a viral-induced event rather than an ubiquitous response to stress in this cellular model as suggested by Fig 4A.

To further investigate a potential interaction between MNV products and G3BP1, we performed an immunoprecipitation assay using MNV-infected cell lysates. G3BP1 is a protein containing several different interaction motifs with proteins and nucleic acids [19, 60] and

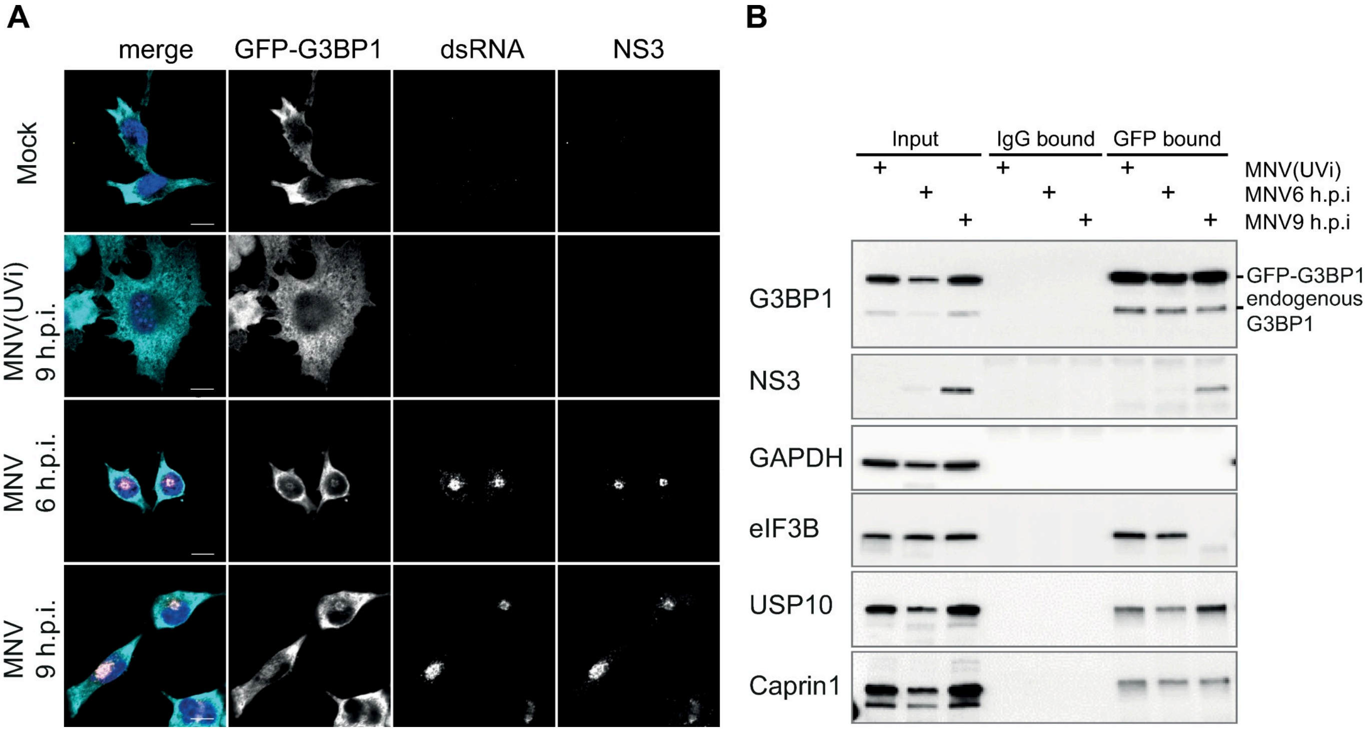

Fig 5. G3BP1 colocalises with MNV replication complex. GFP-G3BP1 colocalises with viral factors in MNV-infected cells (A and B). (A) Mock-, MNV(UV)- or MNV-infected BV2 GFP-G3BP1 cells (MOI 10) were incubated for 6 and 9h p.i prior fixation. Representative view (n = 2) of a confocal analysis of the subcellular distribution of GFP-G3BP1 (cyan), showing MNV replication complexes identified by double immunodetection against dsRNA (magenta) and MNV NS3 (gold). Nuclei were stained with DAPI. Scale bars, 10μm. GFP-G3BP1 co-precipitates with MNV NS3 (B). Representative western blot analysis (n = 3) of a co-immunoprecipitation assay against GFP-G3BP1 (GFP) performed in extracts of cells infected as described above. A parallel co-precipitation using a normal IgG has been used as a control (IgG). Levels of cellular and viral proteins are shown in Inputs, IgG-bound fractions and GFP-bound fractions.

https://doi.org/10.1371/journal.ppat.1008250.g005

known for its ability to homo- and hetero-oligomerize. We addressed G3BP1 interacting partners in BV2 cells expressing GFP-G3BP1 and used an anti-GFP antibody rather than a G3BP1 antibody, allowing us to capture entire G3BP1-containing complexes in cells infected with MNV or MNV(UVi), at 6 or 9h p.i. As shown in Fig 5B, the immunoprecipitation of GFP-G3BP1 led to a strong enrichment of G3BP1 in the GFP-bound fractions for all three conditions but not for the control IgG-bound fractions. The absence of GAPDH in the anti-GFP bound fractions confirms the specificity of the experimental conditions. Paralleling the co-localization of NS3 and G3BP1 seen by confocal microscopy (Fig 4), we observed substantial co-immunoprecipitation of NS3 in the anti-GFP bound fraction at 9h p.i. with MNV. Interestingly, analysis of the known interactors of G3BP1 revealed different patterns of co-precipitation with no significant differences between the MNV(UVi) and the MNV-infected cells for Caprin1 and USP10, and a striking absence of interaction at 9h p.i. for the translation initiation factor eIF3B (Fig 5B). Noteworthy, in the absence of viral stress, G3BP1 is able to interact with its known SG partners USP10, Caprin1 or eIF3B, as previously reported by interactome studies [14, 61], supporting the existence of networks of RBP interactions in the cytoplasm that help nucleate granules when later required. Overall, this supports the previously observed absence of recruitment of eIF3B with G3BP1 foci in MNV-infected cells, and their resistance to CHX treatment observed by confocal microscopy (Fig 4), which could suggest that the re-localization of G3BP1 is independent from the exchange of messenger ribonucleoproteins (mRNPs) with polysomes.

G3BP1 ability to undergo SG-like phase transition is unaffected by MNV

The ability of G3BP1 to undergo LLPT, and drive SG assembly in cells under stress is dependent upon dynamic post-translational modifications. This has been linked in particular to the removal of methyl groups on Arginine residues [62] and the phosphorylation status of the Serine 99 [63]. These modifications prevent unnecessary and untimely formation of G3BP1 aggregates by neutralizing the physical ability of G3BP1 to homo- and hetero-oligomerize with other SG-associated proteins and non-translating RNAs [64]. The ability of G3BP1 to undergo LLPT can by recapitulated *in vitro* by inducing selective condensation of the low-complexity aggregation-prone proteins with biotinylated-isoxazole (b-isox), in conjunction with an EDTA-EGTA lysis buffer releasing transcripts from polysomes [65, 66]. The b-isox-induced aggregates can then be isolated from the soluble fraction by centrifugation, respectively defined as pellet and supernatant.

We therefore addressed the possibility that inhibitory post-translational modifications of G3BP1 in MNV-infected cells prevent LLPT by adding b-isox to cytoplasmic extracts of RAW 264.7 cells, mock- or infected with MNV for 10h (Fig 6A). Quantification of immunoblotting analysis showed no difference in the levels of G3BP1 recovered in the b-isox precipitated fractions (pellets) compared to the inputs in the extracts from mock- or MNV-infected cells (Fig 6B). Moreover, the canonical SG marker Caprin1 and to a lesser extend the 48S component eIF3B and ribosomal protein rpS6 were also precipitated with G3BP1, suggesting both the precipitation of low-complexity proteins and the interaction of G3BP1 with non-translating mRNPs. This may reflect the stabilization or enhancement of preexisting interactions with G3BP1, which drive SG cores assembly [67, 68], confirming an authentic recapitulation of P-eIF2α-dependent SG assembly in this experimental set-up. Conversely, we did not observe precipitation of the viral RNA polymerase NS7 or the replication complex components NS1/2 (Fig 6A and S6A Fig). This suggests that MNV infection does not result in conditions that hinder G3BP1 ability to undergo the LLPT normally associated with the accumulation of SGs. Next, we hypothesized that stimulation of MNV-infected cells with an SG inducer may result in further assembly of canonical SGs. To test this, mock or MNV-infected BV2 cells were treated for 1h with 1μM of the eIF4A inhibitor hippuristanol (Hip), a non-reversible inducer of eIF2α-independent translational shut-off and SG assembly, previously found to inhibit MNV translation [69, 70]. In both mock and MNV-infected cells, hippuristanol treatment resulted in strong accumulation of canonical SGs, containing both eIF3B and G3BP1 (Fig 6C and 6D). Finally, we evaluated the possibility that the relocation of G3BP1 reflects an evasion strategy to escape the assembly of antiviral canonical SG. To this end we induced the formation of SGs prior to infection with MNV and measured viral titre (S6B Fig). SG assembly, stimulated by with hippuristinol, strongly impaired MNV particle production of approximately 100-fold (S6C Fig). These results suggest that SGs may play an antiviral role and thus MNV-driven re-localization of G3BP1 counteracts this cellular response pathway.

Remodeling of G3BP1 interactome during MNV infection

SGs are dynamic membrane-less structures that undergo fusion, fission and move in the cytosol [71]. In addition to mRNAs, RNA-binding proteins and translation factors, different subsets of SGs have been shown to contain specific proteins or mRNAs associated with the specific pathways resulting in their assembly, *i.e* components of the interferon (IFN) signaling pathway during infection or subsets of RBPs during neurodegeneration-associated stress [11]. Recently, an increased understanding of SG biogenesis and function has been achieved by characterizing the RNA and protein composition of SGs in yeast and mammalian cells [14, 15, 61]. These studies relied on affinity enrichment or proximity ligation using G3BP1 as a bait to

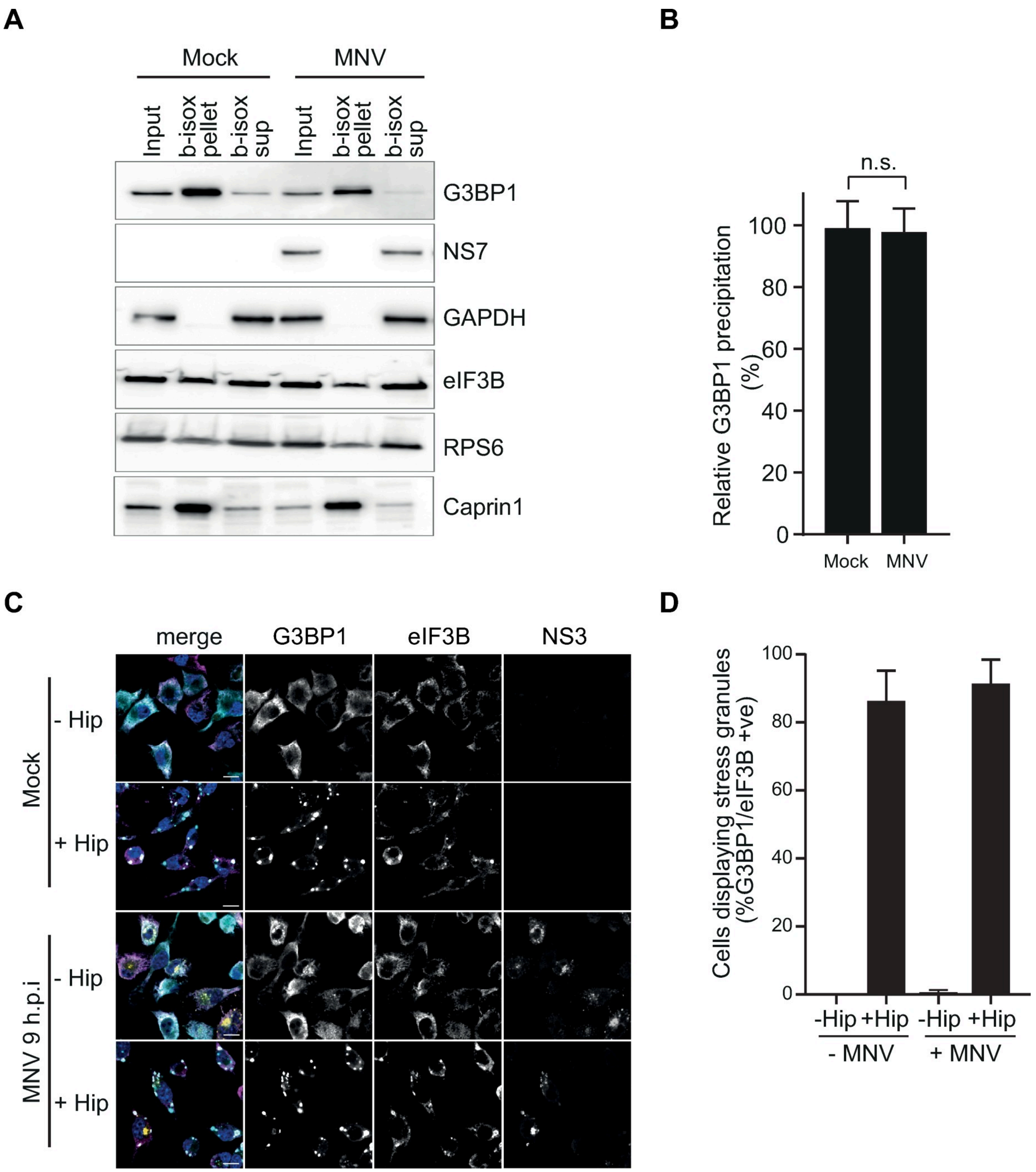

Fig 6. SG formation is not impaired in MNV-infected cells. *In vitro* induced LLPT leads to SG-like aggregates formation in RAW264.7 cells extracts (A and B). Naïve (Mock) or MNV-infected RAW264.7 cells for 10hp.i. (MOI 10) were lysed and *100μM* of b-isox added to the extracts before centrifugal separation between b-isox induced SG-like aggregates (b-isox pellet) and supernatant (b-isox sup). (A) Western blot analysis of the distribution of cellular and viral proteins. For each condition, samples were loaded as Input, b-isox pellet and b-isox supernatant from left to right. (B) Bar plot of the relative G3BP1 precipitation as the ratio between the level of G3BP1 in the b-isox pellet compared to the Input for the Mock (-MNV) and MNV-infected (+MNV) cells, mean ± SD (n = 3). Statistical analysis shown above the plot, n.s., not significant. *In vivo* induction of SG assembly by hippuristanol treatment in MNV-infected cells (C and D). Mock- or MNV-infected BV2 GFP-G3BP1 cells for 9hp.i. (MOI 10) treated with 1μM of Hippuristanol (+Hip) or DMSO (-Hip) for 1h prior fixation. (C) Representative view (n = 2) of a confocal analysis of the formation of Hippuristanol-induced SG in GFP-G3BP1 (cyan) cells stained for the SG marker eIF3B (magenta) and the infection marker MNV NS3 (gold). Nuclei were stained with DAPI. Scale bars, 10μm. (D) Bar plot of the percentage of cells displaying SG (GFP-G3BP1 and eIF3B positive foci) in NS3-negative (-MNV) and positive cells (+MNV), mean (n = 2) ± SD for 100 GFP-positive cells per slide.

https://doi.org/10.1371/journal.ppat.1008250.g006

unravel the SG interactome. Therefore, we reasoned these could be adapted to characterise MNV-induced G3BP1 interactome. To this end, BV2 GFP-G3BP1 cells were either treated with 0.1 mM arsenite for 1h to induce SG assembly or infected with MNV for 9h. G3BP1 interactors and SG cores were then enriched by sequential centrifugation and purified by immunoprecipitation using antibodies to GFP (to trap GFP-G3BP1) or IgG (as a control) followed by pull down with Protein A-conjugated Dynabeads as previously described [72]. Epifluorescence microscopy analysis then confirmed the isolation on anti-GFP beads of SG core or G3BP1 granules, while no granules could be detected in the control IgG immunoprecipitation (Fig 7A). To characterize the identity of G3BP1-interacting partners within these granules, mass spectrometric analysis was performed.

Mass spectrometry analysis identified 791 proteins from arsenite-treated cells and 387 proteins from MNV-infected cells using for the filtering criteria $\geq$1 Log2-fold changes of MS peak areas of immunoprecipitated proteins compared to the respective IgG antibody (S1 Table). First, to ensure that we had successfully isolated SGs, we compared the proteins identified in arsenite-treated BV2 cells (mouse) to those identified in human cells using a similar procedure [15]. This revealed that 66 out of the 791 (this study) or 317 (Jain *et al*, [15]) G3BP1 interactor proteins significantly overlap between SG preparations (S7 Fig; S2 Table; overlap between the two list $p < 3.234e-55$, hypergeometric test). Moreover, analysis of the enriched proteins reveals that arsenite-induced SG in murine cells are significantly enriched, >10 log2 folds above background, in previously identified components of the human SG core such as translation factors (*i.e* eIF2Balpha, eIF2Bepsilon, eIF4E and PABP2), RNA binding proteins (*i.e* PUM3, FMR1, NUFP2, FUS), tRNA synthetases (*i.e* tyrosyl-tRNA synthetase 2, YARS2), ribosomes biogenesis (*i.e* BRX1 and Rrs1), ATPases (*i.e* ATP2B, ATP1A3, RAD50) and RNA or DNA helicases (*i.e* Ddx47, Helz2 and ATRX) (S8 Fig, S3 Table). In a final comparison, we generated a refined list of common SG proteins identified with different experimental approaches, GFP-based immunoprecipitation [15], BirA-FLAG or APEX2-GFP for proximity labelling [14, 61] but all using G3BP1 as bait. We defined this list as "SG cross-core proteins" (S4 Table). The overlap analysis identified 21 proteins which are consistently and significantly enriched by the different experimental strategies across the three studies (Fig 7B). From this list of SG cross-core proteins, we were able to identify a significant enrichment of 18 out of 21 proteins in the arsenite-induced SG proteins we purified (Fig 7C, p value = 1.167e-30). Based on these comparisons, we concluded we were able to purify SG from these murine cells.

In a second experiment, we next compared the G3BP1 interactome generated in MNV-infected cells with the G3BP1 interactome when cells were treated with arsenite. Strikingly, although a significant subset of proteins was enriched in both the treatment (147 proteins, p value = 6.999e-174), demonstrating there are shared interactions with G3BP1 in both conditions. More interestingly, we identified 230 proteins enriched in MNV infected samples and not in the ARS-treated cells; and 644 proteins in arsenite-only (Fig 7D and S2 Table). Comparison of the human SG proteome and G3BP1 interactome in infected cells clearly identified that different families of proteins are enriched (S3 Table). For example, the m6-adenosine reader protein YTHDF3 or ribosomal RNA processing-like RRP1, RRP8, RRP9, Ddx17, Ddx47, Ddx51 and Ddx27, are found in arsenite-treated cells while BST2, an IFN-induced antiviral host restriction factor [73], Rab7a a late endosome-/lysosome-associated small GTPase involved in virus trafficking [74], associated or guanyl-nucleotide exchange factors like Dock11 and Dock2 in response to chemokine signaling [75, 76] were present in MNV-infected cells and absent in arsenite-induced SGs (Fig 8 and S3 Table). The difference in G3BP1 interacting proteins between arsenite and viral infection demonstrates that viral infection leads to a remodelling of the G3BP1 interactome. To address a potential role of these new G3BP1 interactions for MNV replication, we silenced the expression of proteins highly enriched in the

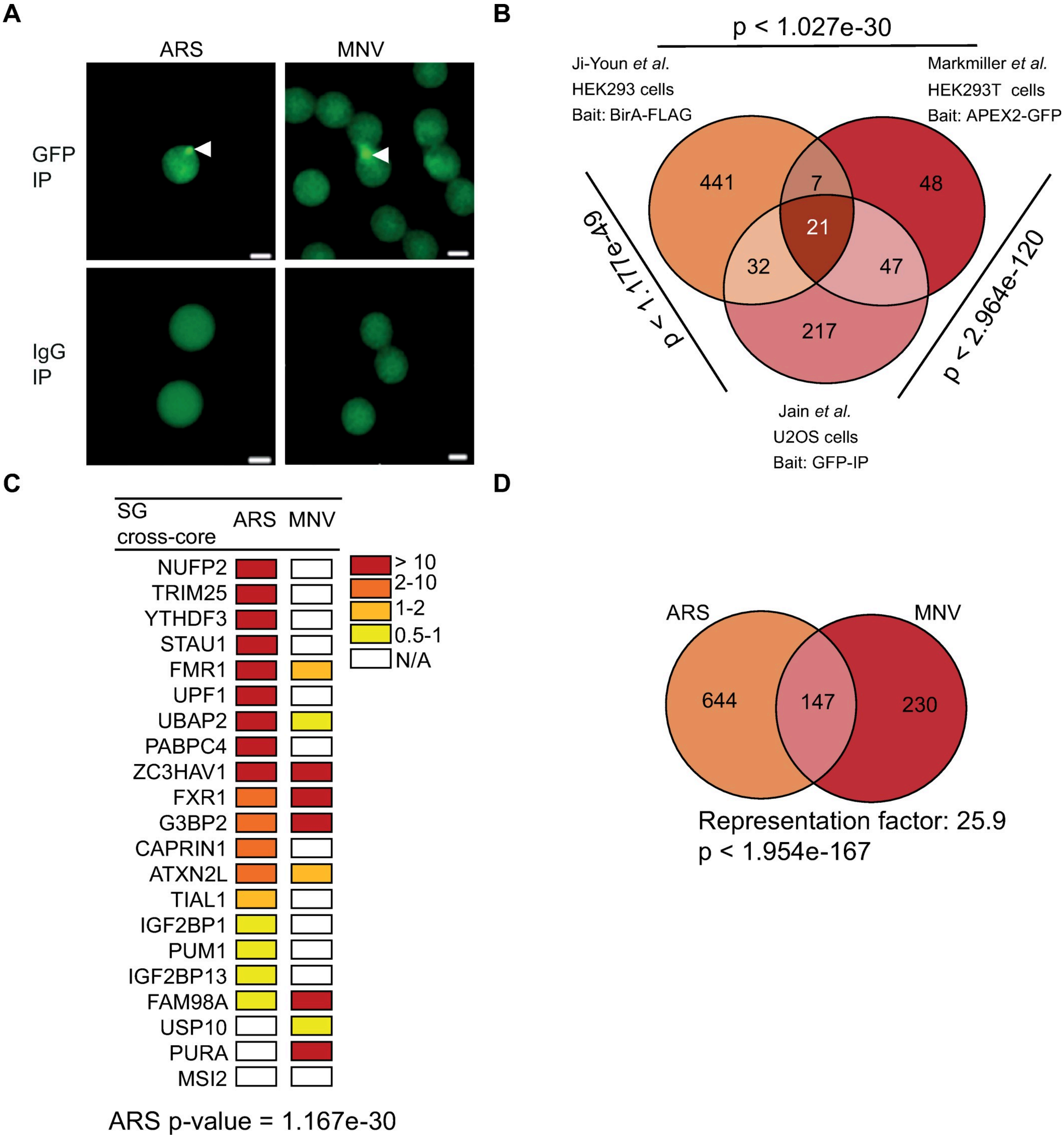

Fig 7. MNV-induced G3BP1 granules are distinct from arsenite-induced stress granules. (A) Dynabeads bound to GFP and to IgG analysed by epifluoresence microscopy in arsenite-stressed and in MNV-infected cells; bead-bound G3BP1 granules are indicated by white arrows (B) Venn diagram of the SGs interactome showing the common elements between three different stress granules (SG) interactome identified in human cells. The hypergeometric p-value is displayed by the side of each group. (C) Heat map representing the 21 proteins identified as "SG cross-core" in arsenite-treated and MNV-infected G3BP1 interactome ranked by the Log2 fold changes. Fold changes are indicated with from red to yellow colour bar and white for N/A. (D) Venn diagram between 795 proteins identified in ARS and 379 in MNV infected cells. The representation factor showed the enrichment over the expected and p-value is based on the cumulative distribution function (CDF) of the hypergeometric distribution of the data set over the mouse proteome.

https://doi.org/10.1371/journal.ppat.1008250.g007

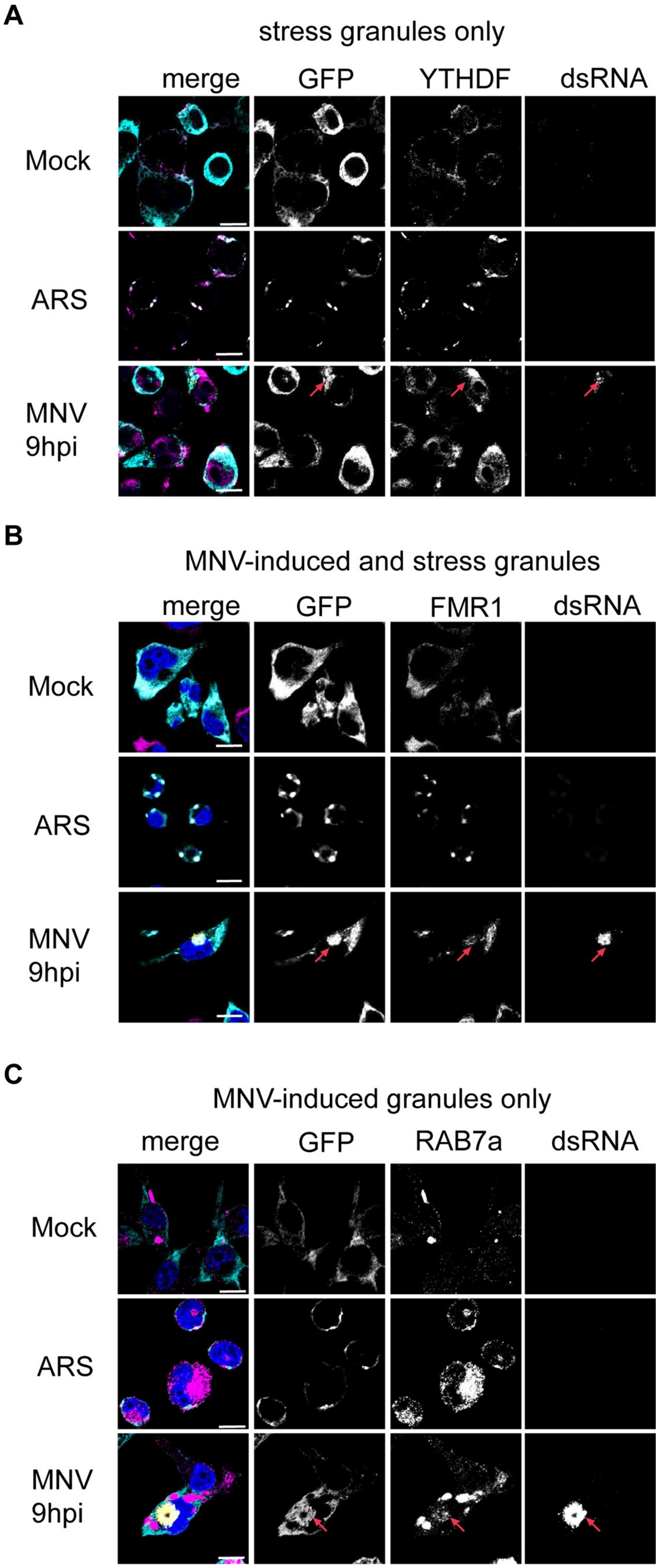
A
stress granules only
merge
GFP
YTHDF
dsRNA
Mock
ARS
MNV
9hpi
B
MNV-induced and stress granules
merge
GFP
FMR1
dsRNA
Mock
ARS
MNV
9hpi
C
MNV-induced granules only
merge
GFP
RAB7a
dsRNA
Mock
ARS
MNV
9hpi

Fig 8. Validation of a non-canonical G3BP1 interactome in MNV-infected cells. G3BP1 interactome differs in MNV-infected cells and arsenite treated cells as addressed by immunofluorescence (A-C). BV2 GFP-G3BP1 cells were either infected with MNV (MOI 10) for 9h p.i. or treated with arsenite 0.1mM for 1h and subcellular colocalisation of candidate proteins identified by mass spectrometry as interacting with GFP-G3BP1 was addressed by immunostaining (magenta) in GFP-G3BP1 positive cells (cyan). MNV-infected cells were detected by immunostaining against dsRNA (gold), nuclei were stained with DAPI. Scale bars, 10μm, red arrows indicate example of colocalisation between GFP-G3BP1 and a candidate protein. Representative view (n = 3) of confocal analysis using staining against (A) YTHDF3, candidate for arsenite-induced SG only, (B) FMR1, candidate for both arsenite- and MNV-induced G3BP1 granules, (C) Rab7, candidate for MNV-induced G3BP1 granules only.

https://doi.org/10.1371/journal.ppat.1008250.g008

MNV-induced G3BP1 interactome using lentiviral shRNA vectors (Rbm25, Rpl7 or Sf3b1) as well as TIAL-1, a scaffolding SG protein that was excluded from this interactome, (S9 Fig). We next evaluated the importance of their reduced expression on MNV replication. While silencing the expression of TIAL-1 had no impact on the level of MNV-1 gRNA, the silencing of Rpl7 or Sf3b1 resulted in significant reduction in MNV-1 gRNA. Silencing of rbm25 had a more variable effect, however, with a similar trend (Fig 9). Thus, this suggests that these proteins, which are components of the remodelled G3BP1 interactome are important during MNV-1 replication. These results altogether clearly support a model in which MNV infection result in a redistribution of G3BP1 cellular protein partners, which may contribute to counteracting the assembly of SGs during infection.

Discussion

In the present study, we have addressed how murine norovirus, a positive strand RNA virus, evades the host anti-viral response in macrophages cell lines and immortalized cells by investigating step-by-step and challenging the activation of the ubiquitous axis P-eIF2α–SG assembly. Despite what could be seen as manifest hallmarks of induction of this classical anti-viral response during MNV infection (Fig 1), we have demonstrated the absence of canonical SG formation and, oppositely, the recruitment of the canonical SG marker G3BP1 to replication complexes (Fig 4). Moreover, proteomic analysis of MNV-induced G3BP1 interactome showed a composition drastically different from that found in arsenite-induced SG in BV2 cells (Fig 7), further demonstrating the unique nature of such complexes.

In addition to the known levels of control by post-translational modifications, the ability of G3BP1 to nucleate SGs has been linked to its interaction with either Caprin1 or USP10 competing for the NTF2 motif on G3BP1 in a mutually exclusive manner, where USP10 plays an inhibitory anti-aggregation role [60]. The switch between USP10 and Caprin1 binding modifies the physical properties of G3BP1, allowing interaction with translationally inactive mRNA through binding to the 40S subunits of stalled initiating transcripts and culminates by the nucleation of SGs by LLPT [60]. Notably, a mimicry of the inhibitory G3BP1-USP10 interaction has been described during infection by old world alphaviruses, preventing the formation of SGs by G3BP1 sequestration and involving FGDF motifs in the viral protein nsp3 [77]. No such motifs had been identified in MNV proteins and as human and murine G3BP1 NTF2 motifs are identical, this seems to rule out a similar mechanism of G3BP1 sequestration during MNV infection. Furthermore, we observed that only a fraction of the cellular G3BP1 seems aggregated and redistributed during MNV replication, suggesting that enough G3BP1 would be available for SG assembly (Figs 2 and 4A). Supporting this hypothesis, we demonstrated that G3BP1 extracted from MNV-infected cells has the physical properties to undergo a LLPT and to form SG-like granules (Fig 6). Moreover, challenging MNV-infected cells with hippuristanol resulted in the assembly of canonical SGs. Thus, the condensation of G3BP1 during infection does not seem responsible for preventing SG formation by sequestering G3BP1, as opposed to what happens during alphavirus replication. Rather, we hypothesize that the

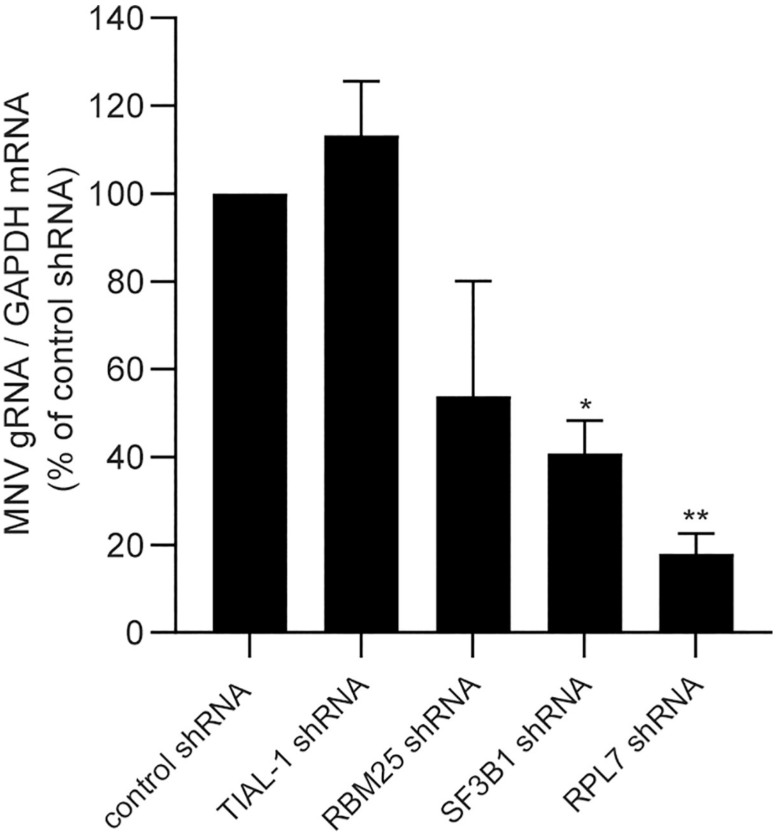

Fig 9. Silencing of the remodelled G3BP1 partners impacts on MNV replication. Transient silencing of factors interacting with G3BP1 in MNV-infected cells lead to a decreased viral replication. BV2 cells were transduced with lentiviral particles carrying shRNA coding sequence for 48h prior MNV infection at MOI 10 and total RNA extracted at t = 0 and 9h p.i. qRT-PCR results show the mean ± SD (n = 3) level of MNV genomic RNA at 9h p.i,. normalised by the level of GAPDH mRNA and presented as percentage of the control shRNA in cells silenced for TIAL-1, Rbm25, SF3B1 and RPL7. Statistical significance given above the bars, *, *P* <0.05, **, *P* <0.01, n.s.

https://doi.org/10.1371/journal.ppat.1008250.g009

signaling trigger required to mediate canonical SG assembly is absent or disabled during MNV infection.

In contrast to the dogmatic understanding of the virus-induced and PKR-dependent P-eIF2α signaling leading to the accumulation of stalled initiating transcripts, and culminating in the assembly of SG [78], we observed an uncoupling between P-eIF2α and the inhibition of translation in MNV-infected cells. We show that both the chemical inhibition of P-eIF2α downstream signaling, using ISRIB, or a cellular model expressing a non-phosphorylatable form of eIF2α, could not rescue the MNV-induced translational shut-off (Figs 2 and 3), excluding a P-eIF2α dependent inhibition of translation and the subsequent accumulation of stalled initiating transcripts [78]. Moreover, MNV infection and arsenite treatment led to similar levels of eIF2α phosphorylation suggesting that there should be enough P-eIF2α to inhibit eIF2B and regulate the host initiation of translation (S5 Fig), which further supports a viral antagonism strategy at the eIF2α signaling nexus. This is reminiscent of the uncoupling of translational suppression from cellular stress responses observed during flavivirus infection, with the difference that DENV and ZIKV infection antagonize eIF2α phosphorylation [79]. Since flavivirus and MNV infection results in the activation of the p38-Mnk1 signaling cascade to regulate eIF4E activity, and PABP activity for MNV, and given that both flavivirus and calicivirus translation are driven by cap-independent translation mechanisms, we propose that the suppression of the host translation by targeting the cap-binding complex, rather than through eIF2α activity, could confer a selective advantages to maintain viral translation in conditions where global translation is impaired [37, 40, 45, 79, 80]. Noticeably, it has also been reported that some forms of stress lead to a phosphorylation of eIF2α correlating with only moderate translation shut-off and without any SG formation [53, 54]. The authors identified the eIF2α kinase GCN2, potentially activated downstream of the translation shut-off itself and remarkably reversing the causality relationship between P-eIF2α and translation inhibition. By analogy, using pharmacological inhibition and genetic deletion we demonstrated that the phosphorylation of eIF2α is indeed dependent upon GCN2 activity (Fig 7F and 7G). Because viruses are obligate intracellular parasites, it is thus tempting to speculate that the translation shut-off occurs as a result of a cellular status of starvation likely generated by the exponential and unchallenged synthesis of viral proteins, rather than through sensing of intermediates of replication and genomic RNA. Furthermore, there are few reported cases of GCN2 activation by viruses, which overall seems to restrict the viral fitness in *in vivo* studies [81]. As MNV virion production does not seem to be affected by ISRIB (S5 Fig) and GCN2 inhibition had no effect on the synthesis of viral non-structural protein (Fig 7F and 7G), it seems quite unlikely that the phosphorylation of eIF2α by GCN2 had any antiviral effects, at least *in vitro*, nor it being repurposed for MNV replication. During the preparation of this manuscript a similar study analyzing stress responses during MNV infection was published by Fritzlar *et al* [82]. Our two studies are in partial agreement. For example, both demonstrate that MNV replication results in a host translational shut-off that is uncoupled from the cellular stress responses. In addition, we agree that MNV replication results in re-localization of G3BP1 into replication complexes. However, some discrepancy merits discussion. Notably, Fritzlar *et al* showed that during infection the kinase PKR is responsible for eIF2α phosphorylation using the pharmacological inhibitor C16. In contrast, we demonstrate that the robust genetic knock-out of GCN2, or pharmacological inhibition of GCN2 are sufficient to abolish eIF2α phosphorylation during MNV infection. These data support that, at least within our experimental conditions, the kinase GCN2 is responsible for MNV-induced eIF2α phosphorylation.

It has been published that a non-replicative MNV RNA transfected into cells does not trigger a PKR-dependent signaling [83], our results would also suggest that the amplification of dsRNA seems to stay surprisingly unnoticed by this particular pattern recognition receptor, at least in our infection model. Previous electron microscopy imaging of cryosections of MNV-infected RAW264.7 cells highlighted that MNV dsRNA and the RNA polymerase NS7 are located on the cytoplasmic side of MNV-induced vesicles rather than in their lumen, which suggest a cytoplasmic replication available for recognition [56]. In light of our results, several hypotheses as to the nature of MNV strategies of PKR avoidance can thus be proposed by analogy with other classical viral mechanisms, such as "hiding in plain sight" or direct inhibition of the non-self recognition machinery. As PKR has also been described as a transducer of MDA5 dependent anti-viral response beside its eIF2α kinase activity [84], this could also explain the poor interferon response to MNV infection [85]. In particular, this hypothesis would fit the model where the MNV factor VF1 is involved in the antagonism of the IFN response by interaction with the MAVS axis [86] and its activation by MDA5 [87, 88].

Studies aiming at the discovery of the host factors required for MNV replication in murine macrophages cell line BV2 by CRISPR screening showed the requirement of G3BP1 for MNV-induced cell toxicity and replication, suggesting a viral repurpose of this host anti-viral factor [36, 89]. In the present work, we have observed an unexpected spatio-temporal colocalisation of G3BP1 granules with MNV replication complexes by confocal microscopy (Figs 4A and 5A) and a molecular interaction between G3BP1 and viral factor by immunoprecipitation (Fig 5B). The observed pattern of aggregation of G3BP1 fits the subcellular localization of MNV RC described as associated with membranes derived from the secretory pathway and proximal to the microtubule organizing center [56–58]. Interestingly, while MNV infection does not abrogate the ability of G3BP1 to coalesce given the right physico-chemical conditions, no viral factor have been found associated with the *in vitro* condensed SG-like aggregates (Fig 6A) suggesting that the association of G3BP1 with the MNV RC does not result from molecular crowding and LLPT. Finally, the time-dependent increasing recruitment of a fraction of the available cellular G3BP1 concomitant with the accumulation of viral products in the RC (Fig 5A) thus evokes the hijacking of this factor by a stoichiometric type of interaction with either viral proteins or nucleic acids and supports the concept that G3BP1 recruitment to MNV RC is required during the viral life cycle. This is further supported by recent evidence that G3BP1 promotes translation of the VPg-linked RNA and is required for replication of MNV and human norovirus [89].

Recently, the understanding of proteins involved or associated with RNA granules and stress granules in particular has exploded mainly through their biochemical purification, proximity mapping of RNA granules associated proteins or fluorescence-activated particle sorting [14, 15, 61, 90]. To further investigate the evasion of the stress granule response we characterized G3BP1 interactions during MNV infection and compared them to well-characterized arsenite-induced SGs (Fig 7). First, our analysis revealed that arsenite-induced SGs in murine BV2 microglial cells differ in their composition to those assembled in human U2OS or HEK293 cells. However, we recapitulated the enrichment in proteins previously identified as SGs components using similar procedures such as translation factors, RNA binding proteins, tRNA synthetases, ribosomes biogenesis factors, ATPases, RNA or DNA helicases ([15] and S7 Fig). Furthermore, combining the different SGs interactome studies that used G3BP1 as bait to generate a cross-core set of stress granules components revealed that 18 out of 21 of these proteins are enriched in arsenite-induced stress granules isolated from murine cells, confirming the conservation of the interactions across species. In contrast, during MNV infection, only 5 out of 21 of the cross-core stress granules proteins displayed a high enrichment with G3BP1, namely ZC3HAV1, FXR1 and G3BP2. Further analysis of the G3BP1 interactome during infection clearly confirmed a shift in composition with 230 out of 377 proteins associated with G3BP1 specific to MNV infection (Figs 7 and 8 and S2 Table). Of the 147 proteins common with arsenite-induced stress granules, enrichment revealed proteins associated with RNA transport (GO:0051028) and localisation (GO:0006403) and ribonucleoprotein complex biogenesis (GO:0022613) while proteins involved in immune response-regulating cell surface receptor signaling pathway (GO:0002433) and involved in endocytosis (GO:0006897) are associated with MNV-induced granules (S3 Table).

Overall, our results support a model in which MNV infection results in a large cytoplasmic redistribution of G3BP1 partners which, together with the absence of PKR-dependent phosphorylation of eIF2α, could provide the basis for evasion of SG assembly during infection. It also paves the way for further studies investigating how MNV impacts on the global landscape of RBP interactions during infection and how these contribute to viral replication mechanisms.

Materials and methods

Cells, retroviral transduction, gene silencing and MNV-1 production

Murine macrophage cells RAW264.7 (European Collection of Authenticated Cell Cultures ECACC, 91062702) and microglial cells BV2 (American Type Culture Collection, CRL-2467) were maintained in Dulbecco's modified Eagle's medium (DMEM), 4,5g/L D-glucose, Na Pyruvate, L-Glutamine supplemented with 10% foetal calf serum (FCS), 100 U of penicillin/

mL, 100μg of streptomycin/mL, 10mM HEPES, and 2mM L-glutamine (all supplements purchased from Invitrogen) at 37˚C in a 5% CO_2 environment. Primary murine bone marrow derived macrophages (BMDMs) were prepared as described in [91] from C57BL/6 mice bones (kind gift of Dr Christos Gkogkas, The University of Edinburgh) and cultivated in the same medium supplemented with 50ng/ml of M-CSF (Preprotech). BV2 GFP-G3BP1 Puro, BV2 mCherry-eIF3E Neo, BV2 GFP-G3BP1/mCherry-eIF3E Puro/Neo cells and control cells BV2 Neo and BV2 Neo/Puro cells were produced by retroviral transduction of BV2 cells as described in [92]. Transduced cells were selected in complete medium at 2μg/ml of Puromycin (Sigma) or 100μg/ml G418 or 2μg/mL of puromycin and 100μg/ml G418 (Sigma) and propagated in complete medium containing 1μg/mL of puromycin or, 50μg/mL G418 or 1μg/mL of puromycin and 50μg/mL G418. For live-cell imaging, high expressing cells were sorted by flow cytometry. MEFs w.t.-, S51A- and GCN2 $^{-/-}$—CD300lf were produced by retroviral transduction of MEFs w.t. (ECACC, 98061101), S51A (kind gift from M. Coldwell, University of Southampton) and MEFs GCN2 $^{-/-}$ (Kind gift of R. Wek, Indiana University) with the lentiviral particles containing the full-length CD300lf sequence and hygromycin resistance gene, selected at 100μg/ml of hygromycinB (Sigma) and propagated in complete medium containing 50μg/ml of hygromycinB. Silencing of gene expression in BV2 cells was performed using MISSION shRNA lentiviral vectors from Sigma: shRNA RBM25 (SHCLNG-NM_027349), shRNA TIAL-1 (SHCLNG-NM_009383), shRNA SF3B1 (SHCLNG-NM_031179), shRNA Rpl7 (SHCLNG-NM_011291) and non-target control shRNA (SHCLNG-NM_019472) in the pLKO.1-puro vector backbone. Briefly, bacterial glycerol stocks were plated and a single colony amplified in Terrific Broth (TB-Sigma) supplemented with 100 μg/ml of carbenicillin (Sigma) before purification using the Plasmid Maxikit (Qiagen). Lentiviral particles were then produced as described in [92] and reverse transcriptase activity (pU/μl) was measured in the supernatants using the SG-PERT assay as described previously [93]. Silencing was performed by reverse transduction of 1.25x10^5 BV2 cells inoculated with 10^8 pU of lentiviral particles, plated in 12wells plate and incubated for 8h before replacing the inoculum by 2 ml of complete medium. After 48h, the cells were either lysed with 300 μl of RNA lysis buffer (Zymo Research) or infected with MNV at MOI 10 for a further 9h and subsequently lysed for RNA extraction. RNA purification was performed using the Zymo Research kit according to the manufacturer's instructions before reverse transcription using the Precision nanoScript2 Reverse Transcription kit (Primer Design) and polydT primers according to the manufacturer's instructions. Silencing efficiency was measured at 48h and 57h post-transduction (i.e. 0 and 9h p.i.) by quantification of the transcripts levels of the genes of interest by qPCR and the effect on MNV replication was assessed by qPCR for the MNV gRNA using the Precision Plus 2x qPCR Mastermix (Primer Design), primers described in S5 Table and the Quant Studio 7 Flex (Applied Biosystems). Murine norovirus 1 (MNV-1) strain CW1 was described previously [34] and MNV-NS1/2^{Flag} is described in [94]. MNV-1 was propagated in BV2 cells as described in [41] with an extra step of concentration using Amicon Centrifugal Filters 100k (Millipore). Virus titres were estimated by determination of the $TCID_{50}$ in units per millilitre in RAW264.7 cells and infections were carried at a MOI of 10 unless stated otherwise. The times post-infection refer to the time elapsed following medium replacement after a 1h inoculation period.

SG formation, P-eIF2α induction and drug treatment

Unless otherwise stated SG were induced using arsenite (Sigma) at a final concentration of 0.1mM for 1h at 37˚C except for MEFs (0.5mM for 1h) and the disassembly was forced by adding cycloheximide (Sigma) at 10μg/ml 30min after the arsenite treatment. P-eIF2α independent SG were induced using hippuristanol (Kind gift of J. Pelletier, McGill University) at 1μM for 1h. Phosphorylation of eIF2α was induced either by treatment with arsenite as described above, tunicamycin (Sigma) at 5μg/ml for 6h or by UV irradiation at 20mJ/cm^2 using a Stratalinker 1800 (Stratagene). ISRIB (Sigma) was added to the cells at a final concentration ranging from 10 to 1000nM and A-92 (Axon Medchem) from 100 and 1000nM at t = 0hp.i and for the indicated times.

Immunoblotting

Immunoblotting analysis was performed as described in [41]. Briefly, approximately 10$^{\wedge 6}$ BV2 cells or BMDMs, 2x10$^{\wedge 6}$ RAW264.7 cells or 5.10$^{\wedge 5}$ MEF cells were plated onto 35mm dishes and infected the next day with MNV at a MOI of 10 as described above. At the indicated times, cells were lysed in 150μL of 1x Gel Loading Buffer (New England Biolabs), sonicated and boiled 5min at 95˚C. Cell lysates were separated by SDS-PAGE, using 10μg of total proteins, and transferring the proteins to nitrocellulose or polyvinylidene difluoride membranes. These were then probed with the following primary antibodies: rabbit anti-eIF2α (1:1,000, Cell Signaling), mouse anti-P-eIF2α (1:5,000, Invitrogen), goat anti-eIF3B (1:2,000, Santa Cruz), rabbit anti-NS3 (1:1,000, kind gift from I. Goodfellow), rabbit anti-NS7 (1;10,000), rabbit anti-G3BP1 (1:2,000, Sigma), rabbit anti-Caprin1 (1:1,000, Bethyl Laboratories), rabbit anti-USP10 (1:1,000, Bethyl Laboratories), rabbit anti-rpS6 (1:1,000, Cell Signaling), mouse anti-GAPDH (1:20,000, Invitrogen); followed by incubation with the appropriate peroxidase labelled secondary antibodies (Dako) and chemiluminescence development using the Clarity Western ECL Substrate (Bio-Rad). The results were acquired using the VILBER imaging system. Phostag analysis was performed to detect mobility shift of phosphorylated eIF2α as described in [79]. Briefly, 2x10$^{\wedge 6}$ RAW264.7 cells were scraped on ice at different times post infection, pelleted for 2min at 4˚C full speed, washed in PBS and lysed in 125μl of cold Lysis Buffer (Tris HCl pH 7.4 50mM, NaCl 150mM, Triton X100 1%) supplemented with antiphosphatase and antiprotease cocktails (Roche). Lysates were incubated for 30min on ice before being centrifuged at 13K rpm for 30min at 4C and the supernatants transferred to new Eppendorf tubes. Protein concentrations were measured by BCA (Pierce) according to the manufacturer's instructions. Twenty-five μg of total proteins were denatured 3min at 95˚C and loaded onto Mn^{2+}-Phos-tag SDS-PAGE gel prepared as described in [50, 51]. Both basal and phosphorylated forms of eIF2α were visualised using an antibody anti-eIF2α. Signal was detected using the Advance ECL Chemocam Imager (Intas Science Imaging) and band quantified using Lab-Image 1D Software (Intas Science Imaging).

Immunofluorescence microscopy

10$^{\wedge 6}$ BV2 cells and BMDMs or 2x10$^{\wedge 6}$ RAW264.7 cells were plated on glass coverslips in a 6 wells plate, 5x10$^{\wedge 5}$ MEF w.t. and S51A were plated on poly-L-Lysine coated glass coverslips according to the manufacturer instructions (Sigma). Cells were infected the next day with MNV at MOI of 10 for the indicated times, fixed with a solution of 4% PFA (Sigma) in PBS for 30min at room temperature (RT), washed in PBS and store at 4˚C. After permeabilisation with 0.1% Triton-X100 (Sigma) in PBS for 5min at RT and 3 washes with PBS, the coverslips were blocked with 0.5% BSA (Fisher) in PBS for 1h at RT then incubated with 200μl of primary antibodies solution for 2h at RT. After 3 washes with PBS, coverslips were incubated in the dark with 200μl of fluorescently-labelled secondary antibodies solution containing 0,1μg/mL DAPI solution (Sigma). The coverslips were then washed and mounted on slides with a drop of Mowiol 488 (Sigma). Confocal microscopy was performed on a Ti-Eclipse—A1MP Multiphoton Confocal Microscope (Nikon) using the Nikon acquisition software NIS-Elements AR. Primary antibodies dilutions: rabbit anti-NS3 (1:600), mouse anti-dsRNA (1:1,000), mouse anti-puromycin (1:5, http://dshb.biology.uiowa.edu/PMY-2A4), mouse anti-G3BP1 (1:400, Invitrogen), goat anti-eIF3B (1:400, Santa Cruz), rabbit YTHDF3 (1:600, Proteintech), rabbit anti-RAB7A (1:600, Proteintech), rabbit anti-FMR1 (1:600, Novusbio). Secondary antibodies were all purchased from Invitrogen: goat anti-rabbit Alexa 488, goat anti-mouse Alexa 555, chicken anti-mouse Alexa 488, donkey anti-goat Alexa 555 and chicken anti-rabbit Alexa 647. All quantification analysis were made using Image J software package Fiji (http://fiji.sc/wiki/index.php/Fiji) and all images were processed using the Nikon analysis software NIS-Element AR.

Ribopuromycylation assay and quantification of fluorescence intensities

Quantification of *de novo* protein synthesis was performed as described by [43]. Briefly, cells were plated on coverslip in 6 wells plate and infected the next day with MNV at MOI of 10 for the indicated times. Prior fixation, all cells were treated with 10μg/ml of puromycin (Sigma), except MEFs treated with 1μg/ml, for 2 min at RT to label the nascent polypeptide chains before addition of 180μM of emetin (Sigma) to block the translation elongation with a further incubation of 2 min at 37˚C. Coverslips were washed 3 times in prewarmed complete medium, fixed with 1ml of 4% PFA in PBS for 15min at RT, washed 3 times in PBS. Cells treated with 100μg/mL cycloheximide for 5 min prior to puromycylation were used as control. Cells treated with 5μg/mL tunicamycin for 6h prior to puromycylation were used as a control of P-eIF2α-dependent inhibition of translation. Fluorescence intensities were quantified by using Image J software package Fiji as described in [79].

Live-cell imaging

MNV-1 was produced has described above except BV2 cells were cultivated in microscopy medium (phenol red free DMEM, 4,5g/L glucose supplemented with 10% FCS, 100U/ml of penicillin, 100μg/mL of streptomycin, 10mM HEPES, and 2mM L-glutamine and 1x Na Pyruvate (Invitrogen)).

$10^{\wedge 5}$ BV2 GFP-G3BP1/mCherry-eIF3E Neo Puro cells were seeded on 12-well glass-bottom plates (Cellvis) in 2ml microscopy medium (phenol red free DMEM, 4,5g/L glucose, HEPES, L-glutamine (Invitrogen) supplemented with 10% FCS, 100U/ml of penicillin, 100μg/mL of streptomycin). Cells were infected with MNV-1 at a MOI of 20 and directly transferred for live-cell imaging. Images were acquired with a 40x magnification (Nikon objective CFI P-Fluor 40x N.A. 1.30 oil immersion) every 15 min for 20 h using an UltraVIEW VoX Spinning Disk Confocal Microscope from PerkinElmer (Volocity software package) and a Hamamatsu Orca Flash 4 camera.

Biotin-isoxazole (b-isox) induction liquid-liquid phase transition

Treatment were performed as described in [66]. Briefly, $2x10^{\wedge 7}$ RAW264.7 cells were plated onto 10cm dishes, Mock or MNV-infected the next day at a MOI of 10 and further cultivated for 10h post infection (p.i). The dishes were placed on ice and washed with cold PBS (from 10x solution–Lonza) and the cells lysed on ice with 1ml of EE buffer (Hepes pH 7.4 50mM, NaCl 200mM, Igepal 0.1%, EDTA pH8 1mM, EGTA pH8 2.5mM, Glycerol 10%, DTT 1μM supplemented with RNAsin (Promega) and anti-protease cocktail (Roche)). Lysates were transferred to a 1.5ml Eppendorf and incubated with agitation for 20min at 4˚C before being spun down at 13,000 rpm 15min at 4˚C. 50μl of the supernatant was kept as "input", mixed with an equal volume of 2x Loading buffer (Cell Signaling) and boiled at 95˚C for 5min. The remaining supernatant was supplemented with 100μM of b-isox (Sigma) and the precipitation reactions were carried out for 90min at 4˚C with agitation. Aggregates were pelleted down by centrifugation at 10,000xg for 10min at 4˚C. 50μL of the supernatant was kept as "soluble fraction", mixed with an equal volume of 2x loading buffer and boiled at 95˚C for 5min. The pellets were washed twice with 500μL of cold EE buffer, spin down at 10,000g 10min at 4˚C, resuspended into 200μL of 1x Gel Loading Buffer (New England Biolabs) as "insoluble fraction" and boiled at 95˚C for 5min.

Immunoprecipitation

10^7 BV2 GFP-G3BP1 cells were plated onto 10cm dishes, infected the next day with MNV or MNV(UV) at a MOI of 10 and further cultivated for 6 and 9hp.i. The dishes were placed on ice and washed twice with cold PBS (from 10x solution–Lonza) and the cells lysed on ice with 500μL of cold Lysis Buffer (Tris-HCl pH7.4 50mM, NaCl 50mM, $MgCl_2$ 15mM, CHAPS 0.12% (w/v), RNAsIn (Promega) 200u/ml, DTT 2mM, Beta-Glycerophosphate 1,75mM, NaF 50mM, NaPyrophosphate 2mM, antiprotease cocktail (Roche). Lysates were incubated 30min on ice, centrifuged at 2krpm, 2min at 4˚C, the supernatant transferred to a new Eppendorf tube and flash frozen in liquid nitrogen. 25μL of magnetic Sepharose-Protein G beads (Invitrogen) per sample were washed twice in cold PBS and incubated overnight in IP buffer (Tris-HCl pH7.4 50mM, NaCl 100mM, $MgCl_2$ 15mM, yeast tRNA 100μg/mL, BSA 5ug/mL, RNAsin 200u/mL (Promega) DTT 2mM, antiprotease cocktail (Roche) at 4˚C with either 0.5μg of anti-GFP antibody (Invitrogen, Monoclonal mAb 3E6) or 0.5μg of normal mouse IgG (Santa Cruz). The beads were washed 3 times in IP buffer, resuspended in 250μL of IP buffer before adding 250μg of lysate at 1mg/ml to each tube. The IgG-beads:lysates mixes were incubated for 1hr at 4˚C on a rotary wheel, washed 3 times in IP buffer before being resuspended into 100μL of 1x Gel Loading Buffer (New England Biolabs), boiled at 95C for 5min and the supernatants transferred to new Eppendorf.

G3BP1 interactome

9x10^6 BV2 GFP-G3BP1 Puro cells were infected with MNV (MOI 10 for 9h) or stressed with arsenite (0.1mM for 1h) then were crosslinked with 1% formaldehyde in PBS for 10 min at RT, and quenched by adding 125mM of glycine for 10 minutes at RT. The cells were spun at 4˚C for 5 minutes at 230xg and the pellet was re-suspended in 1ml of SG lysis buffer (50mM Tris-HCl pH 7.4, 100mM Potassium Acetate, 2mM Magnesium Acetate, 0.5mM DTT, 50μg/mL Heparin, 0.5% NP-40, 1 complete mini EDTA-free protease inhibitor tablet (Roche)) and then lysed by passing through a 25G 5/8 needle seven times on ice and spun at 1,000xg for 5 minutes. The supernatant was collected and spun down at 18,000xg for 20 min at 4˚C. Subsequently the supernatant was removed and the pellet was re-suspended in 1mL of SG lysis buffer and again spun down at 18,000xg for 20 min at 4C. Finally the pellet was re-suspended in 300μL of SG lysis buffer (stress granule core enriched fraction) and nutated at 4˚C for 1hr with 60μl of magnetic Dynabeads Protein A (Invitrogen). Once the beads have been removed, the supernatant was incubated with specific antibody (1μg of rabbit anti-GFP antibody and 1μg of IgG) and nutated overnight at 4˚C. The unbounded antibody was removed by centrifugation at 18,000xg for 20 min at 4˚C, and the pellet was re-suspended in 300μL of SG lysis buffer before to incubate it with 60μL of Dynabeads Protein A at 4˚C for 3h. The Dynabeads were then washed for 2 min at 4˚C with 1mL of wash buffer 1 (SG lysis buffer and 2M Urea), for 5min at 4˚C with 1mL wash buffer 2 (SG lysis buffer and 300mM potassium acetate), for 5min at 4˚C with 1mL SG lysis buffer and seven times with 1ml of TE buffer (10mM Tris HCl pH 8.0, 1mM EDTA pH 8.0). Mass spectrometric analysis by LC-MS Orbitrap of the Dynabeads was performed at the Proteomics Facility at University of Bristol as detailed in the Supplementary Data.

Statistical analyses

Statistical analysis were performed by using the GraphPad Prism software. Statistical significances were calculated by performing a two-tailed Student's t test (****, $p<0.0001$, ***, $p<0.001$, **, $p<0.01$, n.s., not significant).

Accession numbers

The mass spectrometry proteomics data have been deposited to the ProteomeXchange Consortium via the PRIDE [95] partner repository with the dataset identifier PXD011956.

Supporting information

S1 Text. Supplementary materials and methods.
(DOC)

S1 Fig. The P-eIF2α signaling inhibitor ISRIB has no effect on MNV replication. Bar plots of the viral titres measured by TCID50 (logarithmic scale) from BV2 cells inoculated with MNV (MOI 1) for 16h in presence of increasing doses of ISRIB from 10nM to 1μM. Mean ±SD (n = 3), statistical analysis given above the bars, n.s, not significant.
(PDF)

S2 Fig. Quantitative analysis of P-eIF2α abundance in MNV-infected RAW264.7 cells by PhosTag. (A) Representative PhosTag acrylamide gel analysis (n = 3) of RAW264.7 cells infected (MOI 10) for the indicated times with replicative MNV (upper panel) or non-replicative virus MNV(UV) (lower panel). Naive cells (Mock) were cultivated in parallel for 10h and arsenite-treated cells were used as control. Lower band, unphosphorylated P-eIF2α, upper band, P-eIF2α. The percentages of P-eIF2α compared to total eIF2α for each sample are given below the blots and plotted in (B) total eIF2α being the sum of the signal intensity of the lower and upper bands in each lane.
(PDF)

S3 Fig. MNV replication is not affected by exogenous expression of SG markers in BV2 cells. (A) Bar plots of the viral titres measured by TCID50 (logarithmic scale) from BV2 cells w.t., Puro, Neo, Puro-Neo, GFP-G3BP1, mCherry-eIF3E and GFP-G3BP1/mCherry-eIF3E inoculated with MNV (MOI 1) for 16h. Mean ±SD (n = 3), statistical analysis given above the bars, n.s, not significant. BV2 GFP-G3BP1 cells were infected with MNV for 9hp.i prior fixation. (B) Representative view of confocal analysis (n = 2) of GFP-G3BP1 subcellular localisation with immunodetection of G3BP1 (magenta) and MNV NS3 (gold). Scale bars, 10μm.
(PDF)

S4 Fig. MNV infection does not trigger the anti-viral SG assembly in cell culture. Cells cultures infected with MNV do not display formation of SG in time course experiments (A and B). MNV-infected BV2 GFP-G3BP1 (MOI 10) were fixed at 2, 4, 6, 8 and 9h p.i. Cells treated with 0.1mM of arsenite for 45min were used as a positive control and both mock- and arsenite-treated cells were grown alongside the MNV-infected cells and fixed at 9h p.i. (A) Representative view (n = 2) of a confocal analysis of the formation of SG by dual detection of GFP-G3BP1 (cyan) and eIF3B by immunofluorescence (magenta). The efficiency of MNV infection and replication was addressed by immunodetection against MNV NS3 (gold). Nuclei were stained with DAPI. Scale bars, 10μm. (B) Bar plot of the percentage of cells displaying SG (GFP-G3BP1 and eIF3B positive foci, grey bars) and MNV-infected cells (NS3 positive, magenta bars), mean ± SD for 100 GFP-positive cells analysed across at least 10 acquisitions.
(PDF)

S5 Fig. Endogenous G3BP1 colocalises with MNV replication complex. Endogenous G3BP1 colocalises *in vivo* with NS3 in MNV-infected cells (A and B). (A) MNV-infected BV2 GFP-G3BP1 (MOI 10) were fixed at 9h p.i. Cells treated with 0.1mM of arsenite for 45min were used as a positive control and both mock- and arsenite-treated cells were grown alongside the MNV-infected cells and fixed at 9h p.i. Representative view of confocal analysis (n = 2) of GFP-G3BP1 subcellular localisation (cyan) with immunodetection of G3BP1 (magenta) and MNV NS3 (gold). Nuclei were stained with DAPI. Scale bars, 10μm. (B) MNV(UV)- or MNV-infected BV2 or BMDM were incubated respectively for 9 and 15h p.i prior fixation. Representative view (n = 3) of a confocal analysis of the subcellular distribution of G3BP1 (magenta), showing MNV replication complexes identified by immunodetection against MNV NS3 (gold). Nuclei were stained with DAPI. Scale bars, 10μm. MNV-induced G3BP1 aggregation is observed in living cells (C). Representative view of a time-lapse acquisition by confocal microscopy of BV2 cells expressing GFP-G3BP1 (cyan) and mCherry-eIF3E (magenta) in culture infected with MNV (MOI 20) at 10h15 p.i. Scale bar, 5μm.
(PDF)

S6 Fig. Anti-viral effect of hippuristanol-induced SG on MNV replication. BV2 GFP-G3BP1 cells were treated with 1μM of hippuristanol or DMSO for 1h prior inoculation with MNV (MOI 1) for 16h (B and C). (B) Representative view (n = 3) of the induction of SG formation in hippuristanol treated cells (Hip) by fluorescence microscopy. (C) Bar plots of the viral titre measured by TCID50 (logarithmic scale) from BV2 GFP-G3BP1 untreated, treated with 1μM of hippuristanol (Hip) or DMSO for 1h prior inoculation with MNV (MOI 1) for 16h. Mean ±SD (n = 3), statistical analysis given above the bars, ** $P < 0.05$.
(PDF)

S7 Fig. Analysis of stress granules components between mouse and human cells. Venn diagram of the SGs interactome showing the common elements between human cells (U2OS cells) and mouse cells (BV2 cells). The hypergeometric p-value and enrichment factor are displayed.
(PDF)

S8 Fig. GO analysis of stress granules components in mouse cells. Cytoscape clustering was performed using ClueGO app based on GO terms (molecular function and biological process) considering two side hypergeometric test and Bonferroni correction p-value<0.005, using GO term fusion and layout "perfused force direct" for a clear representation. The nodes were grouped accordingly to GO terms and the node size corresponds to the significance of each GO term in the network. We arbitrarily added an additional colour pattern to the cluster in order to highlight the difference between the two groups on analysis (ARS and MNV).
(PDF)

S9 Fig. Silencing efficiency in BV2 cells. Transient silencing via lentiviral particles transduction of shRNA. 1.25x10^5 BV2 cells were inoculated with10^8 pU of lentiviral particles for 48 and 57h before total RNA extraction. Representative (average of qPCR repeat ±SD, n = 3) efficiencies of silencing measured by qRT-PCR are shown as the level of the mRNA of interest normalised by the level of GAPDH mRNA and presented as percentage of the control shRNA in cells silenced for TIAL-1, RBM25, RPL7 and SF3B1.
(PDF)

S1 Table. List of G3BP1 interactome identified by Mass spectrometry analysis in BV2 cells. List of the proteins for the 3 biological replicates from arsenite-treated cells (A) and from

MNV-infected cells (B). The filter criteria applied is ≥1 Log2-fold changes of average MS peak areas of respective proteins of the immunoprecipitation over the respective IgG antibody.
(XLSX)

S2 Table. List of proteins used to plot the Venn diagram in S3 Fig and for S4 Fig.
(XLSX)

S3 Table. Meta-analysis of pathways enrichment of G3BP1 granulome in arsenite-induced and MNV infected stress granules. Table of the list of the GO, KEGG, REACTOME and CORUM terms with significant hypergeometric p-value with associated gene name belonging to each category. (A) GO analysis performed from the whole granulome identified in BV2 cells upon arsenite treatment. (B) GO analysis performed from 230 proteins specifically identified in BV2 cells upon MNV infection not present in the granulome upon arsenite stress.
(XLSX)

S4 Table. List of G3BP1 interactome identified from three independent studies. Interactomes: (i) from Ji-Youn et al. the list of 501 proteins was obtained applying an arbitrary cut-off of ≥ 1 Log2 fold change between the (counts in the purification divided by counts in the controls); from Jain et al the list of 317 proteins was selected considering ≥2 fold change spectral counts of stressed over not stressed cells; (iii) from Markmiller et al 123 proteins were identified in HEK293 cells from Log2 H/L ratio.
(XLSX)

S5 Table. List of primers used in this study.
(XLSX)

S1 Movie. MNV-induced G3BP1 aggregation is observed in living cells. Representative view of a time-lapse acquisition by confocal microscopy of BV2 cells expressing GFP-G3BP1 (cyan) and mCherry-eIF3E (magenta) in culture infected with MNV (MOI 20), 0.5 fps, from 9h30 to 11hp.i., scale bars 10μm.
(MOV)

Acknowledgments

The authors wish to thank the members of the Locker laboratory for providing feedback on the manuscript.

Author Contributions

Conceptualization: Michèle Brocard, Ian G. Goodfellow, Nicolas Locker.

Data curation: Valentina Iadevaia, Roy Parker.

Formal analysis: Michèle Brocard, Valentina Iadevaia, Philipp Klein, Glenys Lewis, Jia Lu, Margaret M. Willcocks, Roy Parker, Ian G. Goodfellow, Alessia Ruggieri, Nicolas Locker.

Funding acquisition: Ian G. Goodfellow, Alessia Ruggieri, Nicolas Locker.

Investigation: Michèle Brocard, Valentina Iadevaia, Philipp Klein, Belinda Hall, Glenys Lewis, Jia Lu, Roy Parker, Alessia Ruggieri, Nicolas Locker.

Methodology: James Burke, Roy Parker, Nicolas Locker.

Project administration: Nicolas Locker.

Supervision: Nicolas Locker.

Writing – original draft: Michèle Brocard, Valentina Iadevaia, Belinda Hall, Ian G. Goodfellow, Alessia Ruggieri, Nicolas Locker.

Writing – review & editing: Michèle Brocard, Valentina Iadevaia, James Burke, Roy Parker, Ian G. Goodfellow, Alessia Ruggieri, Nicolas Locker.

References

1. McCormick C, Khaperskyy DA. Translation inhibition and stress granules in the antiviral immune response. Nat Rev Immunol. 2017; 17(10):647–60. https://doi.org/10.1038/nri.2017.63 PMID: 28669985.
2. Piccirillo CA, Bjur E, Topisirovic I, Sonenberg N, Larsson O. Translational control of immune responses: from transcripts to translatomes. Nature immunology. 2014; 15(6):503–11. https://doi.org/10.1038/ni.2891 PMID: 24840981.
3. Walsh D, Mathews MB, Mohr I. Tinkering with translation: protein synthesis in virus-infected cells. Cold Spring Harbor perspectives in biology. 2013; 5(1):a012351. Epub 2012/12/05. https://doi.org/10.1101/cshperspect.a012351 PMID: 23209131.
4. Hoang HD, Graber TE, Alain T. Battling for Ribosomes: Translational Control at the Forefront of the Antiviral Response. J Mol Biol. 2018; 430(14):1965–92. https://doi.org/10.1016/j.jmb.2018.04.040 PMID: 29746850.
5. Lu L, Han AP, Chen JJ. Translation initiation control by heme-regulated eukaryotic initiation factor 2alpha kinase in erythroid cells under cytoplasmic stresses. Mol Cell Biol. 2001; 21(23):7971–80. https://doi.org/10.1128/MCB.21.23.7971-7980.2001 PMID: 11689689; PubMed Central PMCID: PMC99965.
6. Deng J, Harding HP, Raught B, Gingras AC, Berlanga JJ, Scheuner D, et al. Activation of GCN2 in UV-irradiated cells inhibits translation. Curr Biol. 2002; 12(15):1279–86. https://doi.org/10.1016/s0960-9822(02)01037-0 PMID: 12176355.
7. Farrell PJ, Balkow K, Hunt T, Jackson RJ, Trachsel H. Phosphorylation of initiation factor elF-2 and the control of reticulocyte protein synthesis. Cell. 1977; 11(1):187–200. https://doi.org/10.1016/0092-8674(77)90330-0 PMID: 559547.
8. Harding HP, Zhang Y, Ron D. Protein translation and folding are coupled by an endoplasmic-reticulum-resident kinase. Nature. 1999; 397(6716):271–4. https://doi.org/10.1038/16729 PMID: 9930704.
9. Garcia MA, Meurs EF, Esteban M. The dsRNA protein kinase PKR: virus and cell control. Biochimie. 2007; 89(6–7):799–811. https://doi.org/10.1016/j.biochi.2007.03.001 PMID: 17451862.
10. Kedersha N, Anderson P. Stress granules: sites of mRNA triage that regulate mRNA stability and translatability. Biochem Soc Trans. 2002; 30(Pt 6):963–9. https://doi.org/10.1042/bst0300963 PMID: 12440955.
11. Protter DS, Parker R. Principles and Properties of Stress Granules. Trends Cell Biol. 2016. https://doi.org/10.1016/j.tcb.2016.05.004 PMID: 27289443.
12. Van Treeck B, Protter DSW, Matheny T, Khong A, Link CD, Parker R. RNA self-assembly contributes to stress granule formation and defining the stress granule transcriptome. Proc Natl Acad Sci U S A. 2018; 115(11):2734–9. https://doi.org/10.1073/pnas.1800038115 PMID: 29483269; PubMed Central PMCID: PMC5856561.
13. Maharana S, Wang J, Papadopoulos DK, Richter D, Pozniakovsky A, Poser I, et al. RNA buffers the phase separation behavior of prion-like RNA binding proteins. Science. 2018; 360(6391):918–21. https://doi.org/10.1126/science.aar7366 PMID: 29650702; PubMed Central PMCID: PMC6091854.
14. Youn JY, Dunham WH, Hong SJ, Knight JDR, Bashkurov M, Chen GI, et al. High-Density Proximity Mapping Reveals the Subcellular Organization of mRNA-Associated Granules and Bodies. Mol Cell. 2018; 69(3):517–32 e11. https://doi.org/10.1016/j.molcel.2017.12.020 PMID: 29395067.
15. Jain S, Wheeler JR, Walters RW, Agrawal A, Barsic A, Parker R. ATPase-Modulated Stress Granules Contain a Diverse Proteome and Substructure. Cell. 2016; 164(3):487–98. https://doi.org/10.1016/j.cell.2015.12.038 PMID: 26777405; PubMed Central PMCID: PMC4733397.
16. Aulas A, Fay MM, Lyons SM, Achorn CA, Kedersha N, Anderson P, et al. Stress-specific differences in assembly and composition of stress granules and related foci. J Cell Sci. 2017; 130(5):927–37. https://doi.org/10.1242/jcs.199240 PMID: 28096475; PubMed Central PMCID: PMC5358336.
17. Khong A, Matheny T, Jain S, Mitchell SF, Wheeler JR, Parker R. The Stress Granule Transcriptome Reveals Principles of mRNA Accumulation in Stress Granules. Mol Cell. 2017; 68(4):808–20 e5. https://doi.org/10.1016/j.molcel.2017.10.015 PMID: 29129640; PubMed Central PMCID: PMC5728175.

18. Namkoong S, Ho A, Woo YM, Kwak H, Lee JH. Systematic Characterization of Stress-Induced RNA Granulation. Mol Cell. 2018; 70(1):175–87 e8. https://doi.org/10.1016/j.molcel.2018.02.025 PMID: 29576526.

19. Reineke LC, Kedersha N, Langereis MA, van Kuppeveld FJ, Lloyd RE. Stress granules regulate double-stranded RNA-dependent protein kinase activation through a complex containing G3BP1 and Caprin1. MBio. 2015; 6(2):e02486. https://doi.org/10.1128/mBio.02486-14 PMID: 25784705; PubMed Central PMCID: PMC4453520.

20. Poblete-Duran N, Prades-Perez Y, Vera-Otarola J, Soto-Rifo R, Valiente-Echeverria F. Who Regulates Whom? An Overview of RNA Granules and Viral Infections. Viruses. 2016; 8(7). https://doi.org/10.3390/v8070180 PMID: 27367717; PubMed Central PMCID: PMC4974515.

21. Reineke LC, Lloyd RE. Diversion of stress granules and P-bodies during viral infection. Virology. 2013; 436(2):255–67. https://doi.org/10.1016/j.virol.2012.11.017 PMID: 23290869; PubMed Central PMCID: PMC3611887.

22. Lopman BA, Trivedi T, Vicuna Y, Costantini V, Collins N, Gregoricus N, et al. Norovirus Infection and Disease in an Ecuadorian Birth Cohort: Association of Certain Norovirus Genotypes With Host FUT2 Secretor Status. J Infect Dis. 2015; 211(11):1813–21. https://doi.org/10.1093/infdis/jiu672 PMID: 25505295; PubMed Central PMCID: PMC4425937.

23. Karst SM. Pathogenesis of noroviruses, emerging RNA viruses. Viruses. 2010; 2(3):748–81. https://doi.org/10.3390/v2030748 PMID: 21994656; PubMed Central PMCID: PMC3185648.

24. Bartsch SM, Lopman BA, Ozawa S, Hall AJ, Lee BY. Global Economic Burden of Norovirus Gastroenteritis. PLoS One. 2016; 11(4):e0151219. https://doi.org/10.1371/journal.pone.0151219 PMID: 27115736; PubMed Central PMCID: PMC4846012.

25. Pringle K, Lopman B, Vega E, Vinje J, Parashar UD, Hall AJ. Noroviruses: epidemiology, immunity and prospects for prevention. Future Microbiol. 2015; 10(1):53–67. https://doi.org/10.2217/fmb.14.102 PMID: 25598337.

26. Capizzi T, Makari-Judson G, Steingart R, Mertens WC. Chronic diarrhea associated with persistent norovirus excretion in patients with chronic lymphocytic leukemia: report of two cases. BMC infectious diseases. 2011; 11:131. Epub 2011/05/19. https://doi.org/10.1186/1471-2334-11-131 PMID: 21586142; PubMed Central PMCID: PMC3118142.

27. Schwartz S, Vergoulidou M, Schreier E, Loddenkemper C, Reinwald M, Schmidt-Hieber M, et al. Norovirus gastroenteritis causes severe and lethal complications after chemotherapy and hematopoietic stem cell transplantation. Blood. 2011; 117(22):5850–6. Epub 2011/04/14. https://doi.org/10.1182/blood-2010-12-325886 PMID: 21487110.

28. Desselberger U, Goodfellow I. Noroviruses: a global cause of acute gastroenteritis. The Lancet Infectious diseases. 2014; 14(8):664–5. https://doi.org/10.1016/S1473-3099(14)70776-5 PMID: 24981040.

29. Stuart RL, Tan K, Mahar JE, Kirkwood CD, Andrew Ramsden C, Andrianopoulos N, et al. An outbreak of necrotizing enterocolitis associated with norovirus genotype GII.3. The Pediatric infectious disease journal. 2010; 29(7):644–7. Epub 2010/07/01. https://doi.org/10.1097/inf.0b013e3181d824e1 PMID: 20589982.

30. Cadwell K, Patel KK, Maloney NS, Liu TC, Ng AC, Storer CE, et al. Virus-plus-susceptibility gene interaction determines Crohn's disease gene Atg16L1 phenotypes in intestine. Cell. 2010; 141(7):1135–45. Epub 2010/07/07. https://doi.org/10.1016/j.cell.2010.05.009 PMID: 20602997; PubMed Central PMCID: PMC2908380.

31. Bartnicki E, Cunha JB, Kolawole AO, Wobus CE. Recent advances in understanding noroviruses. F1000Res. 2017; 6:79. https://doi.org/10.12688/f1000research.10081.1 PMID: 28163914; PubMed Central PMCID: PMC5270584.

32. Zhang D, Tan M, Zhong W, Xia M, Huang P, Jiang X. Human intestinal organoids express histo-blood group antigens, bind norovirus VLPs, and support limited norovirus replication. Sci Rep. 2017; 7(1):12621. https://doi.org/10.1038/s41598-017-12736-2 PMID: 28974702; PubMed Central PMCID: PMC5626734.

33. Oka T, Stoltzfus GT, Zhu C, Jung K, Wang Q, Saif LJ. Attempts to grow human noroviruses, a sapovirus, and a bovine norovirus in vitro. PLoS One. 2018; 13(2):e0178157. https://doi.org/10.1371/journal.pone.0178157 PMID: 29438433; PubMed Central PMCID: PMC5810978.

34. Karst SM, Wobus CE, Lay M, Davidson J, Virgin HWt. STAT1-dependent innate immunity to a Norwalk-like virus. Science. 2003; 299(5612):1575–8. https://doi.org/10.1126/science.1077905 PMID: 12624267.

35. Wobus CE, Thackray LB, Virgin HWt. Murine norovirus: a model system to study norovirus biology and pathogenesis. J Virol. 2006; 80(11):5104–12. https://doi.org/10.1128/JVI.02346-05 PMID: 16698991; PubMed Central PMCID: PMC1472167.

36. Orchard RC, Wilen CB, Doench JG, Baldridge MT, McCune BT, Lee YC, et al. Discovery of a proteinaceous cellular receptor for a norovirus. Science. 2016; 353(6302):933–6. https://doi.org/10.1126/science.aaf1220 PMID: 27540007; PubMed Central PMCID: PMC5484048.

37. Royall E, Locker N. Translational Control during Calicivirus Infection. Viruses. 2016; 8(4):104. https://doi.org/10.3390/v8040104 PMID: 27104553; PubMed Central PMCID: PMC4848598.

38. Olspert A, Hosmillo M, Chaudhry Y, Peil L, Truve E, Goodfellow I. Protein-RNA linkage and posttranslational modifications of feline calicivirus and murine norovirus VPg proteins. PeerJ. 2016; 4:e2134. https://doi.org/10.7717/peerj.2134 PMID: 27375966; PubMed Central PMCID: PMC4928471.

39. Emmott E, Sweeney TR, Goodfellow I. A Cell-based Fluorescence Resonance Energy Transfer (FRET) Sensor Reveals Inter- and Intragenogroup Variations in Norovirus Protease Activity and Polyprotein Cleavage. J Biol Chem. 2015; 290(46):27841–53. https://doi.org/10.1074/jbc.M115.688234 PMID: 26363064; PubMed Central PMCID: PMC4646915.

40. Emmott E, Sorgeloos F, Caddy SL, Vashist S, Sosnovtsev S, Lloyd R, et al. Norovirus-Mediated Modification of the Translational Landscape via Virus and Host-Induced Cleavage of Translation Initiation Factors. Mol Cell Proteomics. 2017;16(4 suppl 1):S215-S29. https://doi.org/10.1074/mcp.M116.062448 PMID: 28087593; PubMed Central PMCID: PMC5393397.

41. Humoud MN, Doyle N, Royall E, Willcocks MM, Sorgeloos F, van Kuppeveld F, et al. Feline Calicivirus infection disrupts the assembly of cytoplasmic stress granules and induces G3BP1 cleavage. J Virol. 2016. https://doi.org/10.1128/JVI.00647-16 PMID: 27147742.

42. Nathans D. Puromycin Inhibition of Protein Synthesis: Incorporation of Puromycin into Peptide Chains. Proc Natl Acad Sci U S A. 1964; 51:585–92. https://doi.org/10.1073/pnas.51.4.585 PMID: 14166766; PubMed Central PMCID: PMC300121.

43. David A, Dolan BP, Hickman HD, Knowlton JJ, Clavarino G, Pierre P, et al. Nuclear translation visualized by ribosome-bound nascent chain puromycylation. J Cell Biol. 2012; 197(1):45–57. https://doi.org/10.1083/jcb.201112145 PMID: 22472439; PubMed Central PMCID: PMC3317795.

44. Obrig TG, Culp WJ, McKeehan WL, Hardesty B. The mechanism by which cycloheximide and related glutarimide antibiotics inhibit peptide synthesis on reticulocyte ribosomes. J Biol Chem. 1971; 246(1):174–81. PMID: 5541758.

45. Royall E, Doyle N, Abdul-Wahab A, Emmott E, Morley SJ, Goodfellow I, et al. Murine norovirus 1 (MNV1) replication induces translational control of the host by regulating eIF4E activity during infection. J Biol Chem. 2015; 290(8):4748–58. https://doi.org/10.1074/jbc.M114.602649 PMID: 25561727; PubMed Central PMCID: PMC4335213.

46. Sidrauski C, McGeachy AM, Ingolia NT, Walter P. The small molecule ISRIB reverses the effects of eIF2alpha phosphorylation on translation and stress granule assembly. Elife. 2015; 4. https://doi.org/10.7554/eLife.05033 PMID: 25719440; PubMed Central PMCID: PMC4341466.

47. Zyryanova AF, Weis F, Faille A, Alard AA, Crespillo-Casado A, Sekine Y, et al. Binding of ISRIB reveals a regulatory site in the nucleotide exchange factor eIF2B. Science. 2018; 359(6383):1533–6. https://doi.org/10.1126/science.aar5129 PMID: 29599245; PubMed Central PMCID: PMC5889100.

48. Lee AS. Mammalian stress response: induction of the glucose-regulated protein family. Curr Opin Cell Biol. 1992; 4(2):267–73. https://doi.org/10.1016/0955-0674(92)90042-b PMID: 1599691.

49. Jiang HY, Wek SA, McGrath BC, Scheuner D, Kaufman RJ, Cavener DR, et al. Phosphorylation of the alpha subunit of eukaryotic initiation factor 2 is required for activation of NF-kappaB in response to diverse cellular stresses. Mol Cell Biol. 2003; 23(16):5651–63. https://doi.org/10.1128/MCB.23.16.5651-5663.2003 PMID: 12897138; PubMed Central PMCID: PMC166326.

50. Kinoshita E, Kinoshita-Kikuta E, Takiyama K, Koike T. Phosphate-binding tag, a new tool to visualize phosphorylated proteins. Mol Cell Proteomics. 2006; 5(4):749–57. https://doi.org/10.1074/mcp.T500024-MCP200 PMID: 16340016.

51. Kinoshita-Kikuta E, Kinoshita E, Yamada A, Endo M, Koike T. Enrichment of phosphorylated proteins from cell lysate using a novel phosphate-affinity chromatography at physiological pH. Proteomics. 2006; 6(19):5088–95. https://doi.org/10.1002/pmic.200600252 PMID: 16941569.

52. Rabouw HH, Langereis MA, Anand AA, Visser LJ, de Groot RJ, Walter P, et al. Small molecule ISRIB suppresses the integrated stress response within a defined window of activation. Proc Natl Acad Sci U S A. 2019; 116(6):2097–102. https://doi.org/10.1073/pnas.1815767116 PMID: 30674674; PubMed Central PMCID: PMC6369741.

53. Knutsen JH, Rodland GE, Boe CA, Haland TW, Sunnerhagen P, Grallert B, et al. Stress-induced inhibition of translation independently of eIF2alpha phosphorylation. J Cell Sci. 2015; 128(23):4420–7. https://doi.org/10.1242/jcs.176545 PMID: 26493332; PubMed Central PMCID: PMC4712817.

54. Ishimura R, Nagy G, Dotu I, Chuang JH, Ackerman SL. Activation of GCN2 kinase by ribosome stalling links translation elongation with translation initiation. Elife. 2016; 5. https://doi.org/10.7554/eLife.14295 PMID: 27085088; PubMed Central PMCID: PMC4917338.

55. Brazeau JF, Rosse G. Triazolo[4,5-d]pyrimidine Derivatives as Inhibitors of GCN2. ACS Med Chem Lett. 2014; 5(4):282–3. https://doi.org/10.1021/ml500052f PMID: 24900825; PubMed Central PMCID: PMC4027772.

56. Hyde JL, Sosnovtsev SV, Green KY, Wobus C, Virgin HW, Mackenzie JM. Mouse norovirus replication is associated with virus-induced vesicle clusters originating from membranes derived from the secretory pathway. J Virol. 2009; 83(19):9709–19. https://doi.org/10.1128/JVI.00600-09 PMID: 19587041; PubMed Central PMCID: PMC2748037.

57. Hyde JL, Gillespie LK, Mackenzie JM. Mouse norovirus 1 utilizes the cytoskeleton network to establish localization of the replication complex proximal to the microtubule organizing center. J Virol. 2012; 86 (8):4110–22. https://doi.org/10.1128/JVI.05784-11 PMID: 22301146; PubMed Central PMCID: PMC3318650.

58. Doerflinger SY, Cortese M, Romero-Brey I, Menne Z, Tubiana T, Schenk C, et al. Membrane alterations induced by nonstructural proteins of human norovirus. PLoS Pathog. 2017; 13(10):e1006705. https://doi.org/10.1371/journal.ppat.1006705 PMID: 29077760; PubMed Central PMCID: PMC5678787.

59. Kedersha N, Cho MR, Li W, Yacono PW, Chen S, Gilks N, et al. Dynamic shuttling of TIA-1 accompanies the recruitment of mRNA to mammalian stress granules. J Cell Biol. 2000; 151(6):1257–68. https://doi.org/10.1083/jcb.151.6.1257 PMID: 11121440; PubMed Central PMCID: PMC2190599.

60. Kedersha N, Panas MD, Achorn CA, Lyons S, Tisdale S, Hickman T, et al. G3BP-Caprin1-USP10 complexes mediate stress granule condensation and associate with 40S subunits. J Cell Biol. 2016; 212 (7):845–60. https://doi.org/10.1083/jcb.201508028 PMID: 27022092; PubMed Central PMCID: PMC4810302.

61. Markmiller S, Soltanieh S, Server KL, Mak R, Jin W, Fang MY, et al. Context-Dependent and Disease-Specific Diversity in Protein Interactions within Stress Granules. Cell. 2018; 172(3):590–604 e13. https://doi.org/10.1016/j.cell.2017.12.032 PMID: 29373831; PubMed Central PMCID: PMC5969999.

62. Tsai WC, Gayatri S, Reineke LC, Sbardella G, Bedford MT, Lloyd RE. Arginine Demethylation of G3BP1 Promotes Stress Granule Assembly. J Biol Chem. 2016; 291(43):22671–85. https://doi.org/10.1074/jbc.M116.739573 PMID: 27601476; PubMed Central PMCID: PMC5077203.

63. Panas MD, Kedersha N, Schulte T, Branca RM, Ivanov P, Anderson P. Phosphorylation of G3BP1-S149 does not influence stress granule assembly. J Cell Biol. 2019; 218(7):2425–32. https://doi.org/10.1083/jcb.201801214 PMID: 31171631; PubMed Central PMCID: PMC6605800.

64. Matsuki H, Takahashi M, Higuchi M, Makokha GN, Oie M, Fujii M. Both G3BP1 and G3BP2 contribute to stress granule formation. Genes Cells. 2013; 18(2):135–46. https://doi.org/10.1111/gtc.12023 PMID: 23279204.

65. Han TW, Kato M, Xie S, Wu LC, Mirzaei H, Pei J, et al. Cell-free formation of RNA granules: bound RNAs identify features and components of cellular assemblies. Cell. 2012; 149(4):768–79. https://doi.org/10.1016/j.cell.2012.04.016 PMID: 22579282.

66. Panas MD, Kedersha N, McInerney GM. Methods for the characterization of stress granules in virus infected cells. Methods. 2015; 90:57–64. https://doi.org/10.1016/j.ymeth.2015.04.009 PMID: 25896634.

67. Wheeler JR, Matheny T, Jain S, Abrisch R, Parker R. Distinct stages in stress granule assembly and disassembly. Elife. 2016; 5. https://doi.org/10.7554/eLife.18413 PMID: 27602576; PubMed Central PMCID: PMC5014549.

68. Niewidok B, Igaev M, Pereira da Graca A, Strassner A, Lenzen C, Richter CP, et al. Single-molecule imaging reveals dynamic biphasic partition of RNA-binding proteins in stress granules. J Cell Biol. 2018; 217(4):1303–18. https://doi.org/10.1083/jcb.201709007 PMID: 29463567; PubMed Central PMCID: PMC5881506.

69. Chaudhry Y, Nayak A, Bordeleau ME, Tanaka J, Pelletier J, Belsham GJ, et al. Caliciviruses differ in their functional requirements for eIF4F components. J Biol Chem. 2006; 281(35):25315–25. https://doi.org/10.1074/jbc.M602230200 PMID: 16835235.

70. Bordeleau ME, Mori A, Oberer M, Lindqvist L, Chard LS, Higa T, et al. Functional characterization of IRESes by an inhibitor of the RNA helicase eIF4A. Nat Chem Biol. 2006; 2(4):213–20. https://doi.org/10.1038/nchembio776 PMID: 16532013.

71. Kedersha N, Stoecklin G, Ayodele M, Yacono P, Lykke-Andersen J, Fritzler MJ, et al. Stress granules and processing bodies are dynamically linked sites of mRNP remodeling. J Cell Biol. 2005; 169(6):871–84. https://doi.org/10.1083/jcb.200502088 PMID: 15967811; PubMed Central PMCID: PMC2171635.

72. Wheeler JR, Jain S, Khong A, Parker R. Isolation of yeast and mammalian stress granule cores. Methods. 2017; 126:12–7. https://doi.org/10.1016/j.ymeth.2017.04.020 PMID: 28457979.

73. Haga Y, Kanda T, Nakamoto S, Nakamura M, Sasaki R, Wu S, et al. Interferon induces interleukin 8 and bone marrow stromal cell antigen 2 expression, inhibiting the production of hepatitis B virus surface antigen from human hepatocytes. Biochemical and biophysical research communications. 2017; 486 (3):858–63. https://doi.org/10.1016/j.bbrc.2017.03.150 PMID: 28363866.

74. Shivanna V, Kim Y, Chang KO. Ceramide formation mediated by acid sphingomyelinase facilitates endosomal escape of caliciviruses. Virology. 2015; 483:218–28. https://doi.org/10.1016/j.virol.2015.04.022 PMID: 25985440; PubMed Central PMCID: PMC4516657.

75. Gadea G, Blangy A. Dock-family exchange factors in cell migration and disease. Eur J Cell Biol. 2014; 93(10–12):466–77. https://doi.org/10.1016/j.ejcb.2014.06.003 PMID: 25022758.

76. Shulman Z, Pasvolsky R, Woolf E, Grabovsky V, Feigelson SW, Erez N, et al. DOCK2 regulates chemokine-triggered lateral lymphocyte motility but not transendothelial migration. Blood. 2006; 108 (7):2150–8. https://doi.org/10.1182/blood-2006-04-017608 PMID: 16772603.

77. Panas MD, Schulte T, Thaa B, Sandalova T, Kedersha N, Achour A, et al. Viral and cellular proteins containing FGDF motifs bind G3BP to block stress granule formation. PLoS Pathog. 2015; 11(2): e1004659. https://doi.org/10.1371/journal.ppat.1004659 PMID: 25658430; PubMed Central PMCID: PMC4450067.

78. Anderson P, Kedersha N. Stressful initiations. J Cell Sci. 2002; 115(Pt 16):3227–34. PMID: 12140254.

79. Roth H, Magg V, Uch F, Mutz P, Klein P, Haneke K, et al. Flavivirus Infection Uncouples Translation Suppression from Cellular Stress Responses. MBio. 2017; 8(1). https://doi.org/10.1128/mBio.02150-16 PMID: 28074025; PubMed Central PMCID: PMC5225315.

80. Song Y, Mugavero J, Stauft CB, Wimmer E. Dengue and Zika Virus 5' Untranslated Regions Harbor Internal Ribosomal Entry Site Functions. MBio. 2019; 10(2). https://doi.org/10.1128/mBio.00459-19 PMID: 30967466; PubMed Central PMCID: PMC6456755.

81. Berlanga JJ, Ventoso I, Harding HP, Deng J, Ron D, Sonenberg N, et al. Antiviral effect of the mammalian translation initiation factor 2alpha kinase GCN2 against RNA viruses. EMBO J. 2006; 25(8):1730–40. https://doi.org/10.1038/sj.emboj.7601073 PMID: 16601681; PubMed Central PMCID: PMC1440839.

82. Fritzlar S, Aktepe TE, Chao YW, Kenney ND, McAllaster MR, Wilen CB, et al. Mouse Norovirus Infection Arrests Host Cell Translation Uncoupled from the Stress Granule-PKR-eIF2alpha Axis. MBio. 2019; 10(3). https://doi.org/10.1128/mBio.00960-19 PMID: 31213553; PubMed Central PMCID: PMC6581855.

83. Witteveldt J, Blundell R, Maarleveld JJ, McFadden N, Evans DJ, Simmonds P. The influence of viral RNA secondary structure on interactions with innate host cell defences. Nucleic Acids Res. 2014; 42 (5):3314–29. https://doi.org/10.1093/nar/gkt1291 PMID: 24335283; PubMed Central PMCID: PMC3950689.

84. Pham AM, Santa Maria FG, Lahiri T, Friedman E, Marie IJ, Levy DE. PKR Transduces MDA5-Dependent Signals for Type I IFN Induction. PLoS Pathog. 2016; 12(3):e1005489. https://doi.org/10.1371/journal.ppat.1005489 PMID: 26939124; PubMed Central PMCID: PMC4777437.

85. McCartney SA, Thackray LB, Gitlin L, Gilfillan S, Virgin HW, Colonna M. MDA-5 recognition of a murine norovirus. PLoS Pathog. 2008; 4(7):e1000108. https://doi.org/10.1371/journal.ppat.1000108 PMID: 18636103; PubMed Central PMCID: PMC2443291.

86. McFadden N, Bailey D, Carrara G, Benson A, Chaudhry Y, Shortland A, et al. Norovirus regulation of the innate immune response and apoptosis occurs via the product of the alternative open reading frame 4. PLoS Pathog. 2011; 7(12):e1002413. https://doi.org/10.1371/journal.ppat.1002413 PMID: 22174679; PubMed Central PMCID: PMC3234229.

87. Xu LG, Wang YY, Han KJ, Li LY, Zhai Z, Shu HB. VISA is an adapter protein required for virus-triggered IFN-beta signaling. Mol Cell. 2005; 19(6):727–40. https://doi.org/10.1016/j.molcel.2005.08.014 PMID: 16153868.

88. Seth RB, Sun L, Ea CK, Chen ZJ. Identification and characterization of MAVS, a mitochondrial antiviral signaling protein that activates NF-kappaB and IRF 3. Cell. 2005; 122(5):669–82. https://doi.org/10.1016/j.cell.2005.08.012 PMID: 16125763.

89. Hosmillo M, Lu J, McAllaster MR, Eaglesham JB, Wang X, Emmott E, et al. Noroviruses subvert the core stress granule component G3BP1 to promote viral VPg-dependent translation. Elife. 2019; 8. https://doi.org/10.7554/eLife.46681 PMID: 31403400; PubMed Central PMCID: PMC6739877.

90. Hubstenberger A, Courel M, Benard M, Souquere S, Ernoult-Lange M, Chouaib R, et al. P-Body Purification Reveals the Condensation of Repressed mRNA Regulons. Mol Cell. 2017; 68(1):144–57 e5. https://doi.org/10.1016/j.molcel.2017.09.003 PMID: 28965817.

91. Thorne L, Lu J, Chaudhry Y, Goodfellow I. miR-155 induction is a marker of murine norovirus infection but does not contribute to control of replication in vivo. Wellcome Open Res. 2018; 3:42. https://doi.org/10.12688/wellcomeopenres.14188.1 PMID: 29900416; PubMed Central PMCID: PMC5974592.

92. Ruggieri A, Dazert E, Metz P, Hofmann S, Bergeest JP, Mazur J, et al. Dynamic oscillation of translation and stress granule formation mark the cellular response to virus infection. Cell Host Microbe. 2012; 12 (1):71–85. https://doi.org/10.1016/j.chom.2012.05.013 PMID: 22817989; PubMed Central PMCID: PMC3873964.

93. Pizzato M, Erlwein O, Bonsall D, Kaye S, Muir D, McClure MO. A one-step SYBR Green I-based product-enhanced reverse transcriptase assay for the quantitation of retroviruses in cell culture supernatants. J Virol Methods. 2009; 156(1–2):1–7. https://doi.org/10.1016/j.jviromet.2008.10.012 PMID: 19022294.

94. McCune BT, Tang W, Lu J, Eaglesham JB, Thorne L, Mayer AE, et al. Noroviruses Co-opt the Function of Host Proteins VAPA and VAPB for Replication via a Phenylalanine-Phenylalanine-Acidic-Tract-Motif Mimic in Nonstructural Viral Protein NS1/2. MBio. 2017; 8(4). https://doi.org/10.1128/mBio.00668-17 PMID: 28698274; PubMed Central PMCID: PMC5513711.

95. Vizcaino JA, Csordas A, del-Toro N, Dianes JA, Griss J, Lavidas I, et al. 2016 update of the PRIDE database and its related tools. Nucleic Acids Res. 2016; 44(D1):D447–56. https://doi.org/10.1093/nar/gkv1145 PMID: 26527722; PubMed Central PMCID: PMC4702828.